Sudan University of Science and Technology

جامعة السودان للعلوم والتكنولوجيا

College of Graduate Studies

كلية الدراسات العليا

Study of Charge Transition Levels of Intrinsic Defect, Band Gab, and Formation Energy in Barium Fluoride and

Calcium Fluoride

دراسة مستويات انتقال شحنة العيوب الذاتية ونطاق الفجوة وطاقة التكوين في فلوريد الباريوم وفلوريد الكالسيوم

By

Abdelaziz Mohammed Ibraheem

B.Sc. (University of Khartoum, Sudan), M. Sc. (Neelain University, Sudan): A Thesis Submitted for Fulfillment of the Requirements for the Degree of Doctor of Philosophy in Physics

Supervised By

Associate Professor: Mohamed Hassan Eisa Salim

Associate Professor: Ahmed Elhassan Elfaki

August 2016

DEDICATION

This work is dedicated to those whom support and encouraged us throughout

our studies, our parents, our brothers, our sisters and our teachers. This thesis

would be incomplete without a mention of the support given by them.

ACKNOWLEDGMENTS

الخلاصة

هذه الرسالة تختص بدراسة التحليل الوظيفي شبة الموضعي وكثافة الهجين لمستويات انتقال الشحنات للعيوب الاصلية في هيكل كل من فلوريد الباريوم وفلوريد الكالسيوم. حسبت مستويات الانتقال من طاقات التكوين المقابلة لمستوى ذرتين ذواتي عيوب وهما فلوريد الباريوم وفلوريد الكالسيوم.عولجت الاخطاء الناشئة عن تأثيرات حجم خلية صغيرة من خلال استقراء طاقات التكوين لحدود لانهائية لحجم الخلية. استخدم عامل ماكوف باين وعامل المحاذاة للتحقق من موثوقية طريقة الاستقراء.استخدمت الامكانات الكاملة لطريقة الموجات المستوية الممتدة خطيا مع طريقة الجهد التبادلي المعدل لبيك جونسون للتحقق من صحة حجم نطاق الفجوة في حسابات الهجين. حسب مستوى الانتقال اللازم لشحنة سالبة لتنتقل من مكان الى اخرووجد انه يساوي2.77 الكترون فولت تحت مستوى نطاق التوصيل وهذه النتيجة متوافقة تماما مع القيمة التجريبية لنطاق الامتصاص الضوئي لفلوريد الكالسيوم وهي 3.3 الكترون فولت فوق نطاق التوصيل. وجد ان اكثر الذرات ذات العيوب الاصلية استقرارا هي شحنة الباريوم الموجبة والتي طاقة تكوينها تساوي 9.82- الكترون فولت .وجد ان درجات استقرارالشحنات ذات العيوب متوافقة تماما مع التقاربر الحديثة القائمة على المبدأ الاولي للحساب .وجد ان استقرارية الشحنات ذات العيوب في كل من فلوريد الباريوم وفلوريد الكالسيوم متطابقة ودقيقة وصالحة للمقارنة المباشرة مع قيم التجارب.

كل الحسابات والنمذجة في هذه الرسالة تمت بواسطة برنامج الكوانتم اسبريسو.

ABSTRACT

This Thesis study semi local and hybrid density functional analysis of charge transition levels of native defects in BaF_2 and CaF_2 structures. The transition levels was calculated from the formation energies corresponding to two defect charge states. The errors arising from the small super cell size effects have been relieved through extrapolating the formation energies to the limit of infinite super cell size. The reliability of the extrapolation method has been verified through the application of two correction factors: the Makov-Payine factor to correct for the unwanted interaction between image charges in periodic super cell simulations, and the potential-alignment factor to align the valence band edges in defective and bulk super cells. The common error in the band gap inherited to semi local density functional has been accounted for by incorporating the hybrid density functional method, leading to a correct placement of the transition levels within the band gap. The band gap size from hybrid calculation is validated using the full potential, Lineralized Augmented Plane wave method with the Modified-Becke-Johnson exchange potential. The calculated transition level for the anion vacancy was (2.77 eV) below the conduction band, agreeing well with the experimental optical absorption band of (3.3eV) associated with the electron transition from the ground state F-center to the conduction band in CaF_2. The most stable native defect was the charged cation in BaF_2 with formation energy(-9.82 eV). The order of defect stabilities

in our calculation was compatible with recent first-principle report, however, our formation energies are more accurate. Interestingly the cation and anion defect stability order in BaF_2 matches that of CaF_2. Our results are sufficiently accurate and, thus, significant for direct comparison with experiments.

All the calculations and simulations in this thesis were done using Quantum Espresso Simulations Package.

List of Tables

List of Figures

List of Symbols

BFGS	Broyden, Fletcher, Goldfarb and Shannon minimization
BS	Basis Set
BZ	Brillouin Zone
CBM	Conduction band minimum
CI	Configuration Interaction
DFT	Density functional theory
DOS	Density of States
EPR	electron paramagnetic resonance
ESR	electron spin resonance
GGA	Generalized gradient approximation
HK	Hohenberg-Kohn
KS	Kohn-Sham
LAPW	Linearized augmented plane wave
LDA	Local density approximation
PAW	Projector augmented wave method
PP	Pseudopotential
PW	plane wave

VBM	Valence band maximum
XC	Exchange-correlation
ENDOR	Electron Nuclear Double Resonance
FPLAPW	Full-Potential Linearized Augmented Plane-Wave
HF	Hartree-Fock
LCAO	Linear Combination of Atomic Orbitals
LSDA	Local Spin Density Approximation
OLCAO	Orthogonalized Linear Combination of Atomic Orbitals
SCF	Self-Consistent-Field
UHF	Unrestricted Hartree-Fock
UV	Ultraviolet
VB	Valence Band
PBE	Perdew, Burke and Ernzerhof functional
PTM	Pressure-transmitting medium
PW91	Perdew & Wang (1991) functional
PZ	Perdew and Zunger parameterisation of a functional

TABLE OF CONTENT

CHAPTER ONE

BARIUM FLOURIDE (BaF$_2$) AND CALCIUM FLOURIDE (CaF$_2$) ALKALINE-EARTH MATERIAL: STRUCTURE AND PROPERTIES

1.1. Introduction

Barium fluoride and calcium fluoride have a wide band gap (experimentally ~ 10 eV and~ 12 eV respectively [1]) material with interesting intrinsic optical properties. Additionally it has essential properties as an effective member of Alkaline Earth fluorides with important applications in semiconductors physics and other dynamic fields.

In 1983 Barium fluoride (BaF$_2$) was discovered to be a fast inorganic scintillator [2, 3].Recently BaF$_2$ and CaF$_2$ has been the target for many theoretical studies and experimental applications [3, 4], [5, 6]. BaF$_2$ has attracted considerable attention in the field of nuclear physics, high energy physics, and nuclear medicine. This is due to its property as a high density luminescent material which is luminescent at 220nm and 195 nm with a very short decay time, leading to wide range of applications in elementary particle and gamma ray detection. For example BaF$_2$ has super ionic conductivity so it makes it a candidate material for high-temperature batteries, fuel cells, chemical filters and sensors [7]. BaF$_2$ is commonly used in manufacturing optical windows, lenses, and prism. This is due to its range from ultraviolet(UV) to infrared (IR)[8]. Additionally a report by Laurite Laboratory group[9]showed that the quality requirements to the barium fluoride (BaF$_2$) crystals can be determined for purpose of constructing a high precision electromagnetic calorimeter. CaF$_2$ is an important material for the manufacture of lenses used in the photolithography

process involved in microelectronics technology [10]. Also, CaF_2 can be used as a material for radiation detection [11].

1.2 Importance of the study

Further developments in technology require materials with new properties. Measurements of the properties of materials provide a wide variety of information about the fundamental of matter, hence besides their implication in technology and several applications, BaF_2 and CaF_2 has also been investigated numerically. However until currently the first principle calculations in BaF_2 is lacking[4]. Obviously the calculation of defect transition levels in BaF_2 and CaF_2 takes central part in the numerical investigation due to its direct impact on the optical application. This is one of our motivations for the present work which deals with the quantitative calculation, using density functional method (DFT)[12] of charge transition levels of native defects in BaF_2 and CaF_2 . For most of their applications, knowledge about the defect formation energies and transition levels in BaF_2 and CaF_2 plays an important role.

 In the reminder of this subsection we briefly survey some of the first principle calculations in BaF_2 and caF_2 and the related fluoride structure. In this survey we postpone the detailed definition and explanation of the terminologies entailed in the calculation (e.g. GGA, hybrid calculations etc …) to Chapter 2.

1.3 previous work

Detailed DFT investigations of the structure and diffusion of intrinsic defects , adsorbed hydrogen, and water molecules in alkali-earth fluorides, including BaF_2, have been carried out by Foster et al[13] Similar investigation was performed by Shi et al[14], They were used ab initio calculations to investigate the defect Structures and optical properties of alkaline-earth fluorides, such as CaF_2 and BaF_2.

The electronic structures of perfect crystals and slabs, F centers, centers, oxygen and hydrogen impurities, and H centers were calculated. In order to obtain a good theoretical method for further calculations on defective systems, the bulk and electronic properties of CaF_2 and BaF_2 crystals have been calculated by seven different methods. The comparison of these seven types of Hamiltonians shows that the best agreement with the experimental results for the lattice constant, bulk modulus, as well as the band structure, is obtained by the hybrid technique (B3PW).Their calculations on perfect slabs show that the direct optical band gaps for CaF_2 and BaF_2 bulks are narrowed for the (111), (110) and (100) surfaces. The (111) surface energy is the smallest one among these three terminations, indicating that the (111) surface is the most stable one, in good agreement with the available experimental result. The relaxation of F atoms in the upper sublayer of the top surface layer is inwards and is comparable with the experimental results. The data obtained in F-center DFT-B3PW calculations show that an un-paired electron is well localized inside the vacancy (VF); the relaxation of atoms surrounding the F center is small; the creation of a neutral VF in CaF_2 and BaF_2 results in a new F-center defect band located at the point 6.75 eV and 7.01 eV, respectively, above the valence band top.

Recentlythe GW method[15], which is computationally demanding but known for its high accuracy, has been used in combination with DFT to study the one- and two-particle effects in the electronic and optical spectra of BaF_2 and CaF_2. In contrast we used hybrid DFT and TB-mBj correction to GGA for the purpose of correcting the BaF_2 ,CaF_2 band gaps. These methods have accuracy comparable with GW but are less computationally expensive .

The most relevant work to ours, but still lacking accurate determination of the charge transition levels, has been performed by Nywere et al [4].

They have performed ab-initio calculation so the formation and migration energie so intrinsic defects (interstitials, vacancies and Frenkel defects) in barium fluoride. The calculations were performed within density-functional

theory and the generalized-gradient approximation, employing pseudopotentials and a plane-wave basis set. There results agree reasonably well with available experimental data. They are also compatible with calculations and experimental data on calcium fluoride. They found that Frenkel pairs are composed of pairs of charged defects and that their formation energies are 3.44eVand1.88eV for cation and anion,respectively.The lowest barrier for defect migration was found to correspond to the migration of the anion vacancy along the ⟨100⟩ direction (energy barrier of 0.53eV),which compares well with the experimental value of 0.59eV.Cation vacancy migration was instead found to require an energy of at least 2.22eV along the easiest migration path, ⟨100⟩. Here the formation and immigration energies of intrinsic defects in BaF_2 have been determined for the purpose of identifying the most stable defect types at moderate doping levels. The same group[16] has recently also used the first-principles calculations to study the elastic constants of the cubic, orthorhombic and hexagonal phases of BaF_2.

1.4 Objectives of the study

As we mentioned before that Shi et al has calculated the properties of the bulk BaF_2 and CaF_2 and their F center defects using hybrid DFT[17] calculations. However they did not determine the defect transition levels. In our present work we used hybrid DFT and the generalized gradient approximation GGA DFT[18] to quantitatively calculate the defect formation energies and charge transition levels of native defects in BaF_2 and CaF_2. Our method follows Alkauskas et al[19] who used the combination of GGA and hybrid DFT to align the underestimated band gap in GGA calculation with the corrected band gap in the hybrid calculation, leading to a corrected placement of the charge transition levels in the corrected band gap.

1.5 Basic structure of bulk MF_2(M refer to Ba or Ca)

As pointed out in the previous section, the structure of MF_2 has been studied in details by Nywere et al[4] . In our present calculation, we used the 12 atoms cell for MF_2 shown in figure 1.1.which belongs to the fluorite solid phase with cubic structure (Fm-3m space group). As shown in figure 1.1. Twelve atomic positions are generated by translating the base atoms, M at (0.0, 0.0, 0.0), and F at (0.25a, 0.25 a, 0.25 a), with the primitive vectors (0.5 a, 0.5 a, 0.0) , (0.0, 0.5 a, 0.5 a) and (0.5 a, 0.0, 0.5 a) where a is the lattice constant. For defective structure, the interstitial defect prefers the octahedral site (0.5a, 0.5a, 0.5a) as mentioned in [4].

(a)
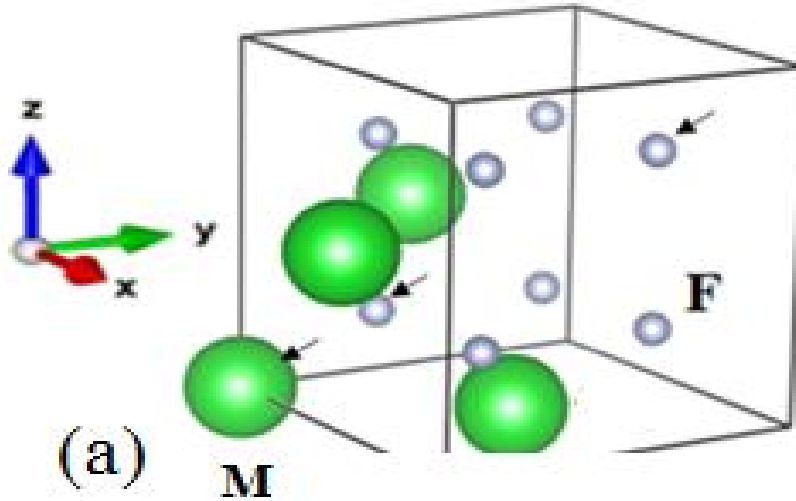
Figure 1.1: The unit cell structure for MF_2 with 12 atoms (4 M and 8 F) used for generating the super cells. The atoms indicated by the arrows form the primitive cell used for obtaining the data.

1.6 Scope of the thesis

This thesis consists of five chapters presented as follows:

Chapter one: concerned with introductions, importance of the study, objectives of the study, and the basic structure of the bulk for Barium fluoride and calcium fluoride. Finally a brief short of the scope of the thesis was been illustrated.

In **chapter two:** a brief overview is given on the DFT calculations (the theoretical method used throughout this thesis) ,beside brief details about the software uses in this thesis .

Chapter three: contains an introduction on different kinds of defects and Impurities in semiconductors, and defects in alkaline- earth fluorides.

Chapter four: concerned with results and discussions

Chapter five: Conclusions of the work carried out together with recommendations for future work is given finally.

CHAPTER TWO

DENSITY FUNCTIONAL THEORY

2.1. Introduction

It has lengthy been well identified that many materials properties are governed through their electronic structure, not too long ago it has turn out to be very convenient to simulate this habits with predictive accuracy. Develops in electronic structure conception, refined software, and development in computer power give an accurate material modeling constitution with suitable prediction of substances properties. Density functional theory (DFT) has become very popular in recent year as a research tool in condensed matter physics, chemistry, material science, and nano science. The Hohenberg-Kohn theorem lays the basis of DFT, it's one procedure that transforms the many -body Schrödinger equation into a much more tractable one–electron equation for numerical solution.

On this chapter, one of the theoretical frameworks which might be used recently for electronic structure calculations within the field of condensed matter is inserted. The major of the Density functional theory (DFT), a quantum mechanical approach for ground state calculations, are defined.DFT is used in this thesis to calculate electronic structure of defects in BaF2.

2.2 The time-independent Schrödinger equation

The time-independent Schrödinger equation for a crystal that illustrate atomic systems can be written as:

$$H\Psi(r_1, r_2, \dots R_1, R_2, \dots) = E\Psi(r_1, r_2, \dots R_1, R_2, \dots) \tag{2.1}$$

where H, E, and Ψ are the Hamiltonian, the electronic energy, and the many-body wave function of the system, and r_i and R_i are the positions ofthe electrons

and ions respectively . The Hamiltonian of the system consisting of nuclei and electrons can is given by:

$$H = -\sum_i \frac{\hbar^2 \nabla_i^2}{2m_e} - \sum_I \frac{\hbar^2 \nabla_I^2}{2M_I} + \frac{1}{2}\sum_{i \neq j} \frac{e^2}{|r_i - r_j|} + \frac{1}{2}\sum_{I \neq J} \frac{Z_I Z_J e^2}{|R_I - R_J|} - \sum_{i,I} \frac{Z_I e^2}{|r_i - R_I|} \qquad (2.2)$$

Where M_I and Z_I are the atomic mass and charge of the nucleus, and e is the electron charge. The first terms is the kinetic energy of the electrons (T_e).And the second term is kinetic energy of nuclei (T_N). The third and forth terms isthe potential energy of Coulomb interaction between electrons (internal potentialV_{int}) and nuclei (V_{II}), respectively, and the last term is the electrons-nuclei Coulomb interactions (external potentialV_{ext}). For curtailment the fundamental Hamiltonian can be written as

$$H = T_e + T_N + V_{int} + V_{II} + V_{ext} \qquad (2.3)$$

On the following discussions we will expose briefly different approximations to solve quantum many-body problem.

2.3 The Born-Oppenheimer approximation

The Born-Oppenheimer approximation is based on the observation that electrons move much faster and weigh much less than the nuclei. It assumes the electronic motion and nuclear motion can be decoupled and that the electrons are in equilibrium with nuclei. This approximation is typically made although not all the methods employ it. In the Born Oppenheimer approximation, the electronic wave function depends on only the nuclear position so the kinetic energy of the nuclei can be neglect in the Hamiltonian. Therefore, electrons has a constant potential energy (V_{II}), and the total electronic Hamiltonian becomes

$$H_{tot} = T_e + V_{int} + V_{II} + V_{ext} \qquad (2.4)$$

In this approximation, the nuclear position is a functional of the electronic wave function, so the electronic Hamiltonian becomes:

$$H_{elec} = T_e + V_{int} + V_{ext} \tag{2.5}$$

and the corresponding Schrödinger equation are:

$$H_{elec}\Psi_{elec}(r_1, r_2, \dots) = E_{elec}\Psi_{elec}(r_1, r_2, \dots) \tag{2.6}$$

We omit explicitly the parametric dependence of Ψ_{elec} on R_I. The totalenergy E_{tot} is then the sum of E_{elec} and the constant nuclear repulsion term E_{nuc}which comes from the constant potential energy V_{II}

$$E_{tot} = E_{elec} + E_{nuc} \tag{2.7}$$

2.4 The Hartree approximation

The HF theory provides approximate solution of the non-relativistic electronic Schrödinger equation. In this approximation the full wave function is assumed to be a product of one electron orbital,

$$\Psi_{elec}(r_1, r_2, \dots, r_n) = \phi_1(r_1)\phi_2(r_2) \dots \phi_n(r_n) \tag{2.8}$$

so each electron moves independently and sees the average potential generated by all the other electrons. From now on Ψ_{elec}will be denoted as Ψ.Thevariational principle in quantum mechanics states that if E_0 is the ground state energy solution of the Schrödinger equation, for any wave function

$$E_0 \leq \frac{\langle \Phi|H|\Phi \rangle}{\langle \Phi|\Phi \rangle} \tag{2.9}$$

Now the Hartree wave function can be used with equation (2.6) and the variational principle to obtain the Hartree equation:

$$\left[-\frac{\nabla^2}{2} - \sum_I \frac{Z_I}{|r_i - R_I|} + + \sum_j \int dr_j \, \Phi_j^*(r_j) \frac{1}{|r_i - R_I|} \phi_j(r_j) \right] \Phi_i(r_i) = \varepsilon_i \Phi_i^*(r_i) \tag{2.10}$$

where each independent electron i feels an effective potential of all electrons by an integration over their densities. Therefore the main many-body equation is

divided into n simpler one-electron equations, and since for each wave function the potential depends on all wave functions, it has to be solved self consistently.

2.5 The Hartree-Fock approximation

The Hartree wave function in equation (2.8) neglects an important property of electrons. It neglects the fact that electrons are Fermi particles, and their wave functions must be anti symmetric with respect to interchanging any pair of particles

$$\Psi(r_1, \ldots, r_k \ldots r_m, \ldots r_n) = -\Psi(r_1, \ldots, r_m \ldots r_k, \ldots r_n) \tag{2.11}$$

The Hartree wave function can be corrected by considering a linear combination of products, and the expression for Fermions can be written as a determinant. For an n-electron system, the Slater determinant is defined as in Ref [17] :

$$\Psi(r_1, r_2, \ldots, r_n) = \frac{1}{\sqrt{n!}} \begin{vmatrix} \phi_1(r_1) & \phi_1(r_2) & \ldots & \phi_1(r_n) \\ \phi_2(r_1) & \phi_2(r_2) & \ldots & \phi_2(r_n) \\ \vdots & \vdots & & \vdots \\ \phi_n(r_1) & \phi_n(r_2) & \ldots & \phi_n(r_n) \end{vmatrix} \tag{2.12}$$

each line of the determinant corresponds to a certain one-electron state, and each column to a certain position in space. The wave function changes sign when two particles (here two rows or columns of the determinant) interchange. Furthermore, if two rows or columns are identical then the determinant equals zero, which means that such a situation (two identical particles occupying the same spatial coordinates) is not physically possible.

Using the Slater determinant with equation (2.6) and the variational principle, the Hartree Fock equation can be derived as:

$$\left[-\frac{\nabla^2}{2} - \Sigma_I \frac{Z_I}{|r_i - R_I|} + + \Sigma_j \int dr_j \ \Phi_j^*(r_j) \frac{1}{|r_i - R_I|} \Phi_j(r_j) \right] \Phi_i(r_i) -$$

$$\Sigma_j \left[\int dr_j \ \Phi_j^*(r_j) \frac{1}{|r_i - r_j|} \Phi_i(r_j) \right] \Phi_j(r_i) = \mathcal{E}_i \Phi_i^*(r_i) \qquad (2.13)$$

This equation has an extra term compared to the Hartree equation. This term is called the exchange potential, since it comes from considering a constraint related to the exchange of particles. The exchange term also cancels an unphysical self-interaction of electrons in the Hartree equation.

2.6 The Hohenberg-Kohn theorems

Density functional theory is based on the two Hohenberg-Kohn (HK) theorems [18] , as follow:

Theorem I :The ground state particle density $n_o(r)$ of a many-body system

Uniquely determines the external potential V_{ext} up to a constant.

Theorem II : The energy functional E[n] can be defined, for any external potential $V_{ext}(r)$ .The global minimum of this functional is the ground state energy, and the density that minimizes the functional is the exact ground state density $n_o(r)$.

It is assumed that there exist two external potentials $V_{ext}(r)$ and $V'_{ext}(r)$ which differ by more than just a trivial constant. Furthermore, the assumption is made, that both potentials give rise to the same electron density $n_o(r)$. Clearly, arising from the nature of $V'_{ext}(r$ in that case there has to be two different Hamiltonians H and H′. Furthermore Ψ and Ψ′, have to be different, since they fulfill different Schrödinger equations. Finally also the energies E_o and E'_o. Associated with the particular wave function differ. Now the two wave functions Ψ and Ψ′ are used as trial functions assuming the other wave function is the ground state wave function. Then the expressions:

$$E_o < \langle \Psi' |H| \Psi' \rangle = \langle \Psi' |H'| \Psi' \rangle + \langle \Psi' |H - H'| \Psi' \rangle \qquad (2.14)$$

$$E_o < E'_O + \int n_o(r)[V_{ext}(r) - V'_{ext}(r)]dr \tag{2.15}$$

Similarly

$$E'_O < \langle\Psi|H'|\Psi\rangle = \langle\Psi|H|\Psi\rangle + \langle\Psi|H' - H|\Psi\rangle \tag{2.16}$$

$$E'_O < E_o + \int n_o(r)[V'_{ext}(r) - V_{ext}(r)]dr \tag{2.17}$$

By summation of (2.15) and (2.17) leads to the obviously contradictory statement

$$E_o + E'_O < E'_O + E_o \tag{2.18}$$

Hence, no two different external potentials $V_{ext}(r)$ can give rise to the same ground state density $n_o(r)$.

The total energy can be written as

$$E_{HK}[n] = T_e[n] + E_{int}[n] + E_{ext}[n] = F_{HK}[n] + \int n(r) V_{ext}(r)dr \tag{2.19}$$

$$E_{HK}[n] = T_e[n] + E_{int}[n] \tag{2.20}$$

Where is F_{HK} the Hohenberg-Kohn functional which is implicates the energies of the electron system. One of the great achievements of Hohenberg-Kohn theorems that it is reformulate the many body problems in terms of density functional.

2.7 The Kohn-Sham equations

In 1965, Kohn and Sham (KS) provide the idea to replace the original many body system of Hohenberg-Kohan with an auxiliary independent particle system [19]. The auxiliary system is to be chosen in a way that the two systems have exactly the same ground state density.Kohan-Sham considered original interacting system with an external potential V_{ext} replaced by non- interacting system with an effective potential V_{KS}. For the auxiliary independent-particle system, the auxiliary Hamiltonian is:

$$H_{KS} = -\frac{1}{2}\nabla^2 + V_{KS}(r) \tag{2.21}$$

For a system with N independent electrons, the ground state is obtained by solving the N one-electron Schrödinger equations

$$\left[-\frac{1}{2}\nabla^2 + V_{KS}(r)\right]\phi_i(r) = \varepsilon_i\phi_i(r) \tag{2.22}$$

Where there is one electron in each of the N of non-interacting orbitals $\phi_i(r)$ with the lowest eigen values ε_i. The density of the auxiliary system is constructed from:

$$n_{KS}(r) = \sum_i^N|\phi_i(r)|^2 = n(r) \tag{2.23}$$

which is subject to the conservation condition:

$$N = \int_V n(r)dr \tag{2.24}$$

The non-interacting independent-particle kinetic energy T_{KS} is given by,

$$T_{KS} = -\frac{1}{2}\sum_i^N\langle\phi_i|\nabla^2|\phi_i\rangle \tag{2.25}$$

Obliviously course, T_{KS} is not equal to the true kinetic energy of the system. Kohn and Sham introducing the following separation of the functional $F_{KS}[n]$

$$F_{KS}[n] = T_{KS}[n] + E_H[n] + E_{XC}[n] \tag{2.26}$$

where $E_{XC}[n]$, the so-called exchange-correlation energy is defined through Eq. (2.26) as:

$$E_{XC}[n] = (T_e[n] - T_{KS}[n]) + (E_{int}[n] - E_H[n]) \tag{2.27}$$

The exchange and correlation energy EXC is the functional that contains everything that is unknown. So from Eq(2.22) V_{KS} is the effective KS potential in which the electrons move, and is given by

$$V_{KS}(r) = V_{ext} + V_H + V_{XC} = -\sum_I\frac{z_I}{|r-R_I|} + \int\frac{n(r')dr'}{|r-r'|} + \frac{\delta E_{XC}[n(r)]}{\delta[n(r)]} \tag{2.28}$$

We now apply the variational principle and ask: what condition must the orbital $\phi_i(r)$ fulfil in order to minimize this energy expression .The resulting equations are the Kohn- Sham equations

$$\left(-\frac{1}{2}\nabla^2 + V_{ext} + V_H + \frac{\delta E_{XC}[n(r)]}{\delta[n(r)]}\right)\phi_i(r) = \varepsilon_i\phi_i(r) \tag{2.29}$$

The Kohn-Sham equations are solved self-consistently as shown in figure2.1.

and the wave functions$\phi_i(r)$ give the electron density through

$$n(r) = \sum_{i=1}^{occupied}|\phi_i(r)|^2 \tag{2.30}$$

2.8 Geometry Optimization

A theorem derived independently by Hellman and Feynman shows that the force on a nucleus can be specified entirely in terms of its interaction with the surrounding charge density [20]. It can be shown that this force theorem also holds in density functional calculations. Once the self-consistent total energy is evaluated, the forces on the nuclei can be computed from the derivative of the total energy with respect to nuclear coordinates [21].The equilibrium or Optimized geometry is thus the set of nuclear positions that minimize these forces. In practice, a force may be computed once a self-consistent total energy is obtained, and this force can then be used to update the nuclear positions, which in turn yields a new KS self-consistency problem to be solved iteratively. Thus geometry optimization can be considered as an "outer loop" to the self-consistent solution of the KS equations.

2.9 The DFT Self-consistency Loop

The KS equations discussed in section 2.7are solved subject to the condition of consistency between the KS potential $V_{KS}(r)$ (equation (2.28)) and electron density (equation (2.28)). The iterative solution to the KS equations, as well as the outer geometry optimization loop, is shown schematically in figure 2.1. An initial approximation to the charge density initializes the loop; this consists of a

linear combination of atomic orbital (LCAO) approximating the KS orbital which yields an electronic charge density. This is then used to calculate a new KS potential. The KS potential is inserted into a KS Hamiltonian which yields a Schrodinger-like KS equation. Matrix diagonalization in the LCAO basis then leads to the solution of the KS equation, yielding a new set of KS orbital which can be used to construct a new charge density. The input and output densities are "mixed" through a linear combination which assists in convergence, and this generates a new input charge density[22,23] for the next iteration. This process is iterated until the input and output densities of a given iteration differ by less than a user-specified threshold, at which point the system is considered self consistent. The total energy can be calculated at self-consistency and hence the ionic forces can be determined, which again can be compared to a force threshold. After calculating the force, the ionic coordinates are updated, typically using variants of the steepest descent method [24]. Once the force is minimized below the specified threshold, desired quantities such as the band structure and density of states can be obtained at the relaxed geometry.

Initial Guess
$$n(\mathbf{r})$$

Calculate Kohn-Sham Potential
$$V_{KS}(\mathbf{r}) = V_{ext}(\mathbf{r}) + V_{Hartree}(\mathbf{r}) + V_{xc}[n]$$

Solve Kohn-Sham Equation
$$\left[-\frac{1}{2}\nabla^2 + V_{KS}(\mathbf{r})\right]\psi_i(\mathbf{r}) = \varepsilon_i\psi_i(\mathbf{r})$$

Calculate Electron Density
$$n(\mathbf{r}) = \sum_{i=1}^{N}|\psi_i(\mathbf{r})|^2$$

No — Self-Consistent?

Yes

Output
Energy, Forces, etc.
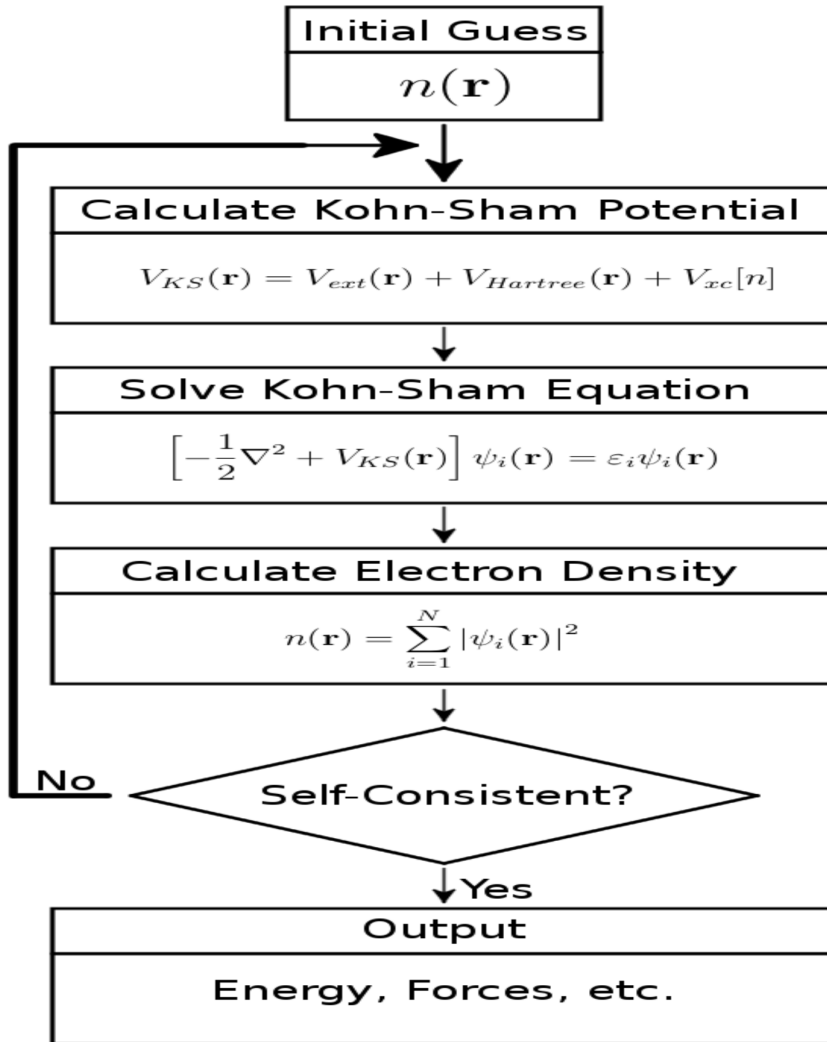
Figure 2.1: Kohn-Sham sow chart. Self-consistency implies either the change in the charge density or the change in the total energy.

2.10 The exchange-correlation functional

The exchange-correlation functional in the Kohn-Sham approach is a priori an unknown functional. However, finding a good, yet simple approximation for the complex exchange-correlation functional is crucial for the correct description of the electronic properties. The success of K-S approach is based on the fact that

the effect of this unknown functional can be approximated very accurately with simple models.

2.10.1 The local density approximation

The approximate exchange-correlation functional originally proposed by Kohn and Sham is the local density approximation (LDA); this is still one of the simplest and effective approximations have been used to date. The LDA assumes that the contribution to the exchange-correlation energy from each point in space is equal to what it would be for a homogeneous electron gas with the same density throughout the whole system as is found at that point; therefore, the functional is local since it only depends on the density at each point independently of the rest of the system. The energy functional is defined as:

$$E_{XC}^{LDA}(n) = \int n(r) \varepsilon_{XC}(n(r)) dr \tag{2.31}$$

Where $\varepsilon_{XC}(n(r))$ is the exchange-correlation energy per particle of a uniform electron gas of density $n(r)$. The quantity $\varepsilon_{XC}(n(r))$ can be further split in to exchange and correlation contributions

$$\varepsilon_{XC}(n(r)) = \varepsilon_X(n(r)) + \varepsilon_C(n(r)) \tag{2.32}$$

ε_{XC} can be derived exactly, whereas ε_C has been found by fitting to quantum Monte-Carlo simulations[25].

The exchange part ε_X, represents the exchange energy of an electron in a uniform electron gas of a particular density, was originally derived by Bloch and Dirac in the late 1920's and it is given by [26].

$$\varepsilon_X = -\frac{3}{4}\left(\frac{3n(r)}{\pi}\right)^{1/3} \tag{2.33}$$

The LDA is very simple; corrections to the exchange-correlation energy due to the in homogeneities in the electronic density are ignored. However it is surprisingly successful and even works reasonably well in systems where the electron density is rapidly varying.

2.10.2 The generalized gradient approximation

The improvements in local density approximation (LDA) by introducing a dependence on the gradient of the electron density($\nabla n(r)$) leads to the generalized gradient approximation (GGAs) for the exchange-correlation which include density gradient corrections and higher spatial derivatives of the electron density and give better results than LDA in many cases. So the XC energy is written as follows

$$E_{XC}^{GGA}(n) = \int n(r)\varepsilon_{XC}(n(r), \nabla n(r))dr \tag{2.34}$$

A large number of good expressions for$E_{XC}^{GGA}(n)$have been proposed and are used within quantum chemistry, materials physics and other areas today. Three most widely used GGAs are the forms proposed by Becke [27], Perdew *et al.*[28], and Perdew, Burke and Enzerhof [29](PBE).

2.11 The band gap problem

If one electron in some state is removed from the system with energy E(N) Where N is number of electron . If one electron is added to the system in the state, the difference between the largest addition energy and the smallest removal energy defines the energy band gap as:

$$I(N) = E(N - 1) - E(N) \; ; A(N) = E(N) - E(N + 1) \tag{2.35}$$

In solids this is the onset of the continuum of optical transitions, if the gap is direct (if the lowest empty state and the highest filled state have the same k vector). From atomic and molecular physics, the highest occupied and lowest unoccupied states are respectively called HOMO (Highest Occupied Molecular Orbital) and LUMO (Lowest Unoccupied MO), while addition and removal energy are respectively called electron affinity A, and ionization potential I. So The fundamental band gap can be defined as the difference between the ionization energy I and the electron affinity A[30] .

$$E_{gab} = I - A \qquad\qquad (2.36)$$

In HF the one-electron energies have the meaning of removal (or addition) energies for extended systems (Koopmans's theorem). If the world were described by single Slater determinants, the difference between the LUMO and HOMO one-electron HF energies would yield the real energy gaps in solids (neglecting polarization effects, i.e. the change in the one-electron states upon addition or removal of an electron). As a matter of facts, experience shows that HF (with the true exchange potential) seriously overestimates the band gap in solid. In DFT, the one-electron energies have acquired a rather bad reputation, mostly due to the failure of KS band gaps (that is: calculated as the difference between LUMO and HOMO KS energies) to reproduce with an acceptable accuracy the true band gap in solids: gaps in DFT are strongly underestimated (up to 50%). This problem is present in both LDA and GGA and is common to HF with Slater's local approximation to exchange. One may say that after all DFT is a ground state theory, and that KS eigen values and eigenvectors are purely mathematical quantities without any physical meaning, but it wouldn't be a very satisfactory answer. In finite systems ionization potentials and electron affinities can be calculated as energy differences between the ground state and a state with one electron added or removed. In extended systems this is of course not possible. The reason for the infamous "band gap problem" lies in

the dependence of the exact energy functional upon the number of electrons and in the in ability of approximate functional to reproduce it. In the next section we consider the extension of DFT to a factionary number of electrons.

2.12 The hybrid functional: an accurate band gap

Without proper corrections of the gap error, electronic properties calculated by pure LDA or GGA are not reliable, thus, cannot be compared to experimental results. In the worst case, defect levels can artificially appear in the band gap or disappear from the band gap leading to qualitatively wrong results. The observation, that LDA or GGA trends are opposite to those of HF, motivated the development of approximations which combine these two approaches, the so-called hybrid functional methods. I mention only the one parameter hybrid functional, which contains a DFT correlation with a combination of DFT and HF exchange in the following form:

$$E_{XC}^{hyb} = \alpha E_X^{HF} + (1 - \alpha)E_X^{GGA} + E_C^{GGA} \tag{2.37}$$

Where E_X^{HF} the exchange energy is calculated with the exact nonlocal HF wave function; E_X^{GGA} and E_C^{GGA} are the conventional semi local GGA exchangeand correlation energies, and α is a mixing parameter. There are several hybrid functional that can be used in different calculations.B3PW91 was the first one introduced in 1993[31] , later in 1994 and1999 the popular B3LYP and PBE0 functional appeared respectively[32,33].In 2003 the screened hybrid HSE06 (Heyd-Scuseria Ernzerhof).

2.13 MBJ lda method

Previously we discuss several approximations which describe properly the band structure of solids. These approximations such as The Local Density Approximation (LDA), the Generalized Gradient Approximation (GGA) , and LSDA+U[34]. Unfortunately they fail among others, describe very well the account for the band gap value of semiconducting based on the use of Green's functions and perturbation theory as the GW approximation, GWA [35, 36], were proposed. In the last ten years, these efforts gave rise to substantially improved results. Some of the new proposals include, the screened hybrid functional of Heyd, Scuseria and Ernzerhof (HSE) [37] and the middle-range exchange and correlation hybrid functional of Henderson, Izmaylov, Scuseria and Saving (HISS)[38] . Another recent proposal is the modified Becke-Johnson potential (mBJLDA) proposed by Tran and Blaha [39]. This potential was introduced to the Wien2k code in 2010. Even with the several theoretical non-properly solved issues, the mBJLDA potential gives rise to acceptable predictions of the band gap value as compared to experiment as it was shown in figure 2.2. If one would prefer to sacrifice a little the precision obtained against the savings in computational cost, the mBJLDA potential seems the appropriate method
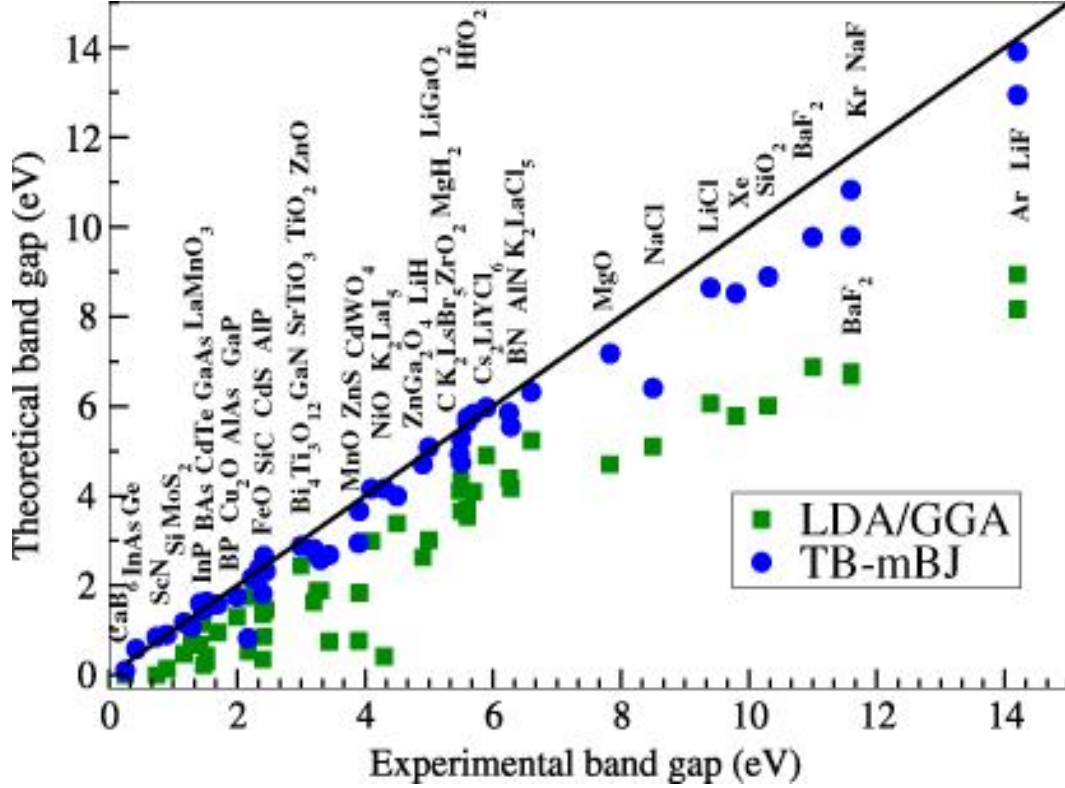
Figure 2.2: show the results obtained with LDA/GGA with Mbj potentials for fundamental band gab for 48 solids using wien2k package [40].

2.14 Bloch theorem and Plane Waves

Expressing the wave function as a sum of plane waves can simplify the computation. In a periodic system Bloch's theorem can be used

$$\varphi_{nk}(r) = e^{iK.r}u_{nk}(r) \tag{2.38}$$

Where $u_{nk}(r)$ a function with the same periodicity as the super cell and k is wave vector representing the position in the Brillouin zone. The complete wave function for state n is given by:

$$\varphi_n(r) = \sum_k \varphi_{n,k}(r) \tag{2.39}$$

The $u_{nk}(r)$ functions can be expanded in a plane wave basis set resulting in the following relation,

$$\varphi_{nk}(r) = \sum_G c_{nk,G}\, e^{i(k+G).r} \tag{2.40}$$

Where G are the reciprocal lattice vectors of the super cell (primitive cell containing the defect, with reduced translation symmetry compared to the host lattice) lattice under consideration. Even though the sum over **G** should be infinite, in practical terms it is truncated to a cutoff value (Gcutoff) and is usually expressed in terms of the boundary equivalent energy *Ecutoff*.

$$\frac{\left|(k+G)^2\right|}{2} < E_{cutoff} \tag{2.41}$$

This boundary is called the energy cut-off and is restricted by replacing an upper boundary to the kinetic energy $\frac{(k+G)^2}{2}$ of the plane waves. The k should also be summed over the entire Brillouin zone. To reduce the computations to a manageable level the wave function is evaluated for a special set of *k*-points that approximate the entire Brillouin zone. In the present study the Monkhorst-Pack scheme is used in which the chosen points form a uniform grid in *k*-space. .

2.15 K-Points

Following on from Bloch's theorem, given that each electron occupies a state of definite k , the infinite number of electrons within the solid gives rise to an infinite number of k-points. At each k-point, only a finite number of the available energy levels will be occupied. Thus one only needs to consider a finite number of electrons at an infinite number of k-points. This may seem to be replacing one infinity (number of electrons) with another one (number of k-points) to little discernible advantage. However, one does not need to consider

all of these k-points ;rather, since the electron wave functions will be almost identical for values of k that are sufficiently close, one can represent the wave functions over a region of reciprocal space by considering the wave function at a single k-point. It is therefore sufficient to consider the electronic states at a finite number of k-points in order to determine the ground state electron density of the solid. The net effect of Bloch's theorem therefore has been to change the problem of an infinite number of electrons to one o f considering only the number of electrons in the unit cell at a finite number of k points chosen so as to appropriately sample the Brillouin zone. An example of where these k-points are can be seen in figure 2.3.
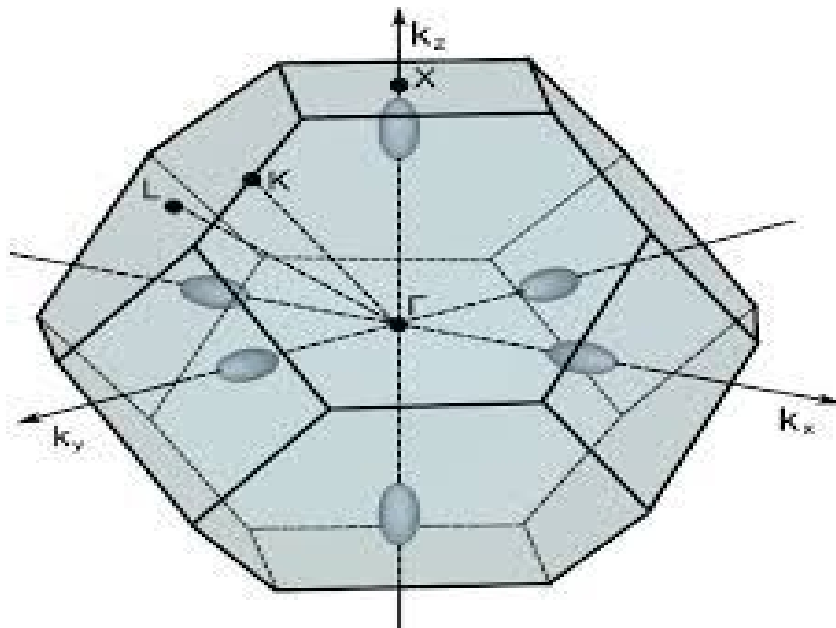
Figure 2.3: Example real-space unit cell and Brillouin zoneatruncated octahedron and can be visualized with eight hexagonal faces and six square faces . The following symmetry points are shown: Γ the point in the center of the zone (origin of k space), X - the point in the middle of square faces, L - the point in the middle of hexagonal faces, and K - the point in the middle of the edge shared by two adjacent hexagons. The directions are: Δ - the axis connecting the Γ and X points,Λ - the axis connecting the Γ and L points, and Σ - the axis connecting the Γ and K points.

K-point sampling of the Brillouin zone is obtained by using a Monkhorst Pack (M-P) grid, which is an unbiased method of choosing a set of k-points[41] An M-P grid is a rectangular grid of points with fractional coordinate dimensions M_x x M_y x M_z spaced evenly throughout the Brillouin zone. The larger the dimensions of the grid, the finer and more accurate will be the sampling.

2.16 Pseudo potentials

One of the main problems encountered when solving the Schrödinger equation numerically for a nuclear potential is that this potential, of the form $-\frac{1}{r}$, is notsmall, and so it is not possible to treat it as a perturbation on the free electron problem, as is done in the nearly-free electron model. This is reflected in the atomic orbital, which decay exponentially as r $\rightarrow \infty$ and oscillate rapidly close to the nucleus in order to maintain orthogonality with each other. The fundamental idea behind the pseudo- potential approximation is to' freeze' the tightly bound core electrons of each atom and replace them with an effective (or pseudo) potential (Ψ_{pseudo}) which attenuates the strong Coulomb potential (V_{pseudo}) close to the nucleus. This approach was first introduced by Hans Hellmann in 1934[42]. It is justified by the fact that the contribution of the core electrons to the total energy, although large, is only very weakly affected by the atom's chemical environment, and so does not play a significant role in its bonding properties; similarly, it is not unreasonable to assume that the core wave functions are unaffected when isolated atoms are brought together. The main advantage of removing the core electrons is to relax the orthogonality constraint they pose on the wave functions of the remaining valence electrons; in fact, these are no longer required to be orthogonal to the core states (although they must still maintain orthogonality with each other), and so can reduce the

41

number of nodes in their radial parts, with the lowest valence state for each angular momentum channel being node less. Therefore, the smooth pseudo potential results in the true valence wave functions being replaced by pseudised wave functions, which vary smoothly in the core region and only match the true ones outside the core radius r_c (see figure 2.4.). The advantage of dealing with a smooth function is obviously a computational one, since this function will be less demanding to approximate accurately with either a truncated basis expansion or a real-space grid representation.
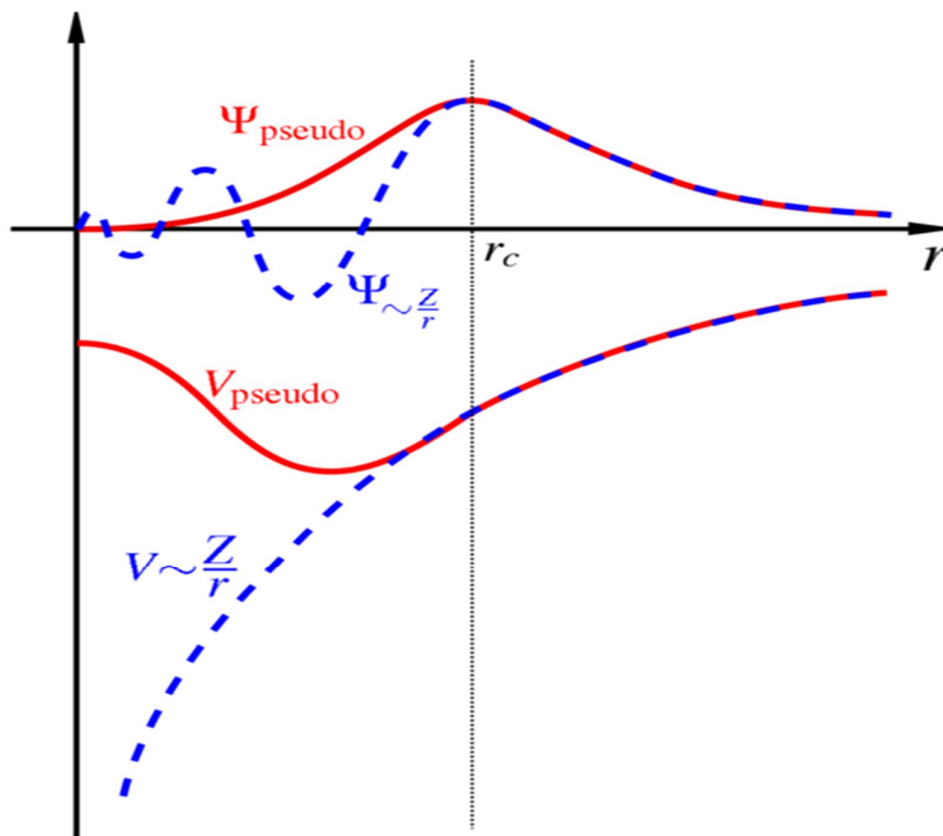
Figure 2.4: .comparison of a wave function in the coulomb potential of a nucleus (blue) to the one in the pseudo potential (red)The pseudised functions are smoother than their true counterparts for r $<r_c$, and match them exactly for r $\geq r_c$.

2.16.1 Ultra soft pseudo potentials

Making the pseudo functions as smooth as possible without losing accuracy is one goal of pseudo potentials, because increasing the smoothness of the pseudo potentials decreases the range in Fourier space necessary to describe the valence properties to a certain accuracy. In Vanderbilt's Ultra soft Pseudo potentials (USPP)[43]. The smoothness of the pseudo functions in comparison to norm-conserving pseudo- potentials is increased by giving up the restriction of norm conservation. This led to much smaller cutoff energies for the expansion of the wave function in k-space resulting in faster computing times while maintaining the desired accuracy.

2.16.2 Projector-augmented waves (PAW)

The projector-augmented wave (PAW) method [44, 45] combines the pseudo potential approach with an all-electron approach. The wave function is parameterized b a pseudo function, but in the core region the pseudized wave function is substituted with the all electron wave function. This combines the great advantages of USPP, namely the reduction of the computational effort with the accuracy of an all electron method.

2.17 Quantum Espresso

Quantum Espresso is a variety of numerical methods & algorithms aimed at a chemically realistic modeling of materials from the nano scale upwards, based on the solution of the density functional theory (DFT).It is an integrated suite of

computer codes for electronic structure calculations and materials modeling based on DFT, plane waves and pseudo potentials(norm conserving, ultra-soft and projector augmented wave) to represent the electron-ion interactions. The ESPRESSO stands for opEn Source Package for Research in Electronic Structure, Simulation &Optimization. The codes are constructed around the use of periodic boundary conditions, which allows for a straightforward treatment of infinite crystalline systems [46].

Quantum espresso can do several important basic computations such as, Calculation of the Kohn-Sham (KS) orbital's and energies for isolated systems, and of their ground state energies, Complete structural optimizations of the atomic coordinates ,ground state of magnetic or spin polarized systems,..etc.

2.18 Choice of Boundary Conditions of DFT

When implementing DFT, the choice of boundary conditions used in the calculations can be very important on the results calculated, as will be seen in many of the proceeding Chapters. There are two options for the treatment, periodic boundaries or boundaries to vacuum, commonly referred to as the super cell or cluster methodologies respectively. In supercell calculations, the modeling is performed within a supercell of tens to hundreds of atoms with periodic boundary conditions that form an infinite perfect crystal in the case of an undistorted super cell. When a defect or defects are introduced into the super cell it forms a periodic array of defects. Super cell calculations have the advantage that defect energies thus calculated are independent of the location of the defect within the super cell. This then gives more reliable results for any calculation involving the comparison of energies of different defect structures, including migration calculations and calculations comparing different structures of the same defect. In cluster calculations, the modeled sample consists of a

nano particle of usually a few hundred atoms, with boundaries to vacuum. The surface bonds of the sample are often terminated with hydrogen atoms to minimize their effect on the calculations. In the cluster, compared with super cell calculations, there are no defect-defect interactions, but instead interactions between the surface of the cluster and the defect within must be considered. Modern computing facilities can allow for the use of large atomic clusters, which can minimize this effect, but defects still need to be kept away from the cluster surface to avoid significant interaction.

Cluster calculations can be more accurate under some conditions than super cell calculations, particularly when dealing with host material for which the LDA band gap underestimation is critical. Quantum confinement in the cluster artificially raises the calculated band-gap of the material, with the gap found to decrease towards the super cell value with increasing cluster size [47]. This effect has been employed to compensate for the LDA band gab underestimation.

CHAPTER THREE

DEFECT AND IMPURITIES IN SEMICONDUCTOR

3.1 Introduction

A perfect crystal is an idealization; there is no such thing in nature. Atom arrangements in real materials do not follow perfect crystalline patterns. Nonetheless, most of the materials that are useful in engineering are crystalline to a very good approximation. There is fundamental physical reason for this. The preferred structures of solids at low temperature are those that minimize the energy. The low-energy atomic configurations are almost invariably crystalline since the regular pattern of the crystal lattice repeats whatever local configuration is most favorable for bonding. There is also a fundamental physical reason why the crystal is imperfect. While a perfect crystalline structure may be preferred energetically, at least in the limit of low temperature, atoms are relatively immobile in solids and it is, therefore, difficult to eliminate whatever imperfections are introduced into the crystal during its growth, processing or use the fact that real materials are not perfect crystals is critical to materials engineering. If materials were perfect crystals then their properties would be dictated by their composition and crystal structure alone, and would be very restricted in their values and their variety. It is the possibility of making imperfectly crystalline materials that permits materials scientists to tailor material properties into the diverse combinations that modern engineering devices require. As we shall see repeatedly in the body of this course, the most important features of the microstructure of an engineering material are the crystalline defects that are manipulated to control its behavior.

It is useful to classify crystal lattice defects by their dimension. The 0-dimensional defects affect isolated sites in the crystal structure, and are hence called point defects. An example is a solute or impurity atom, which alters the

crystal pattern at a single point. The 1-dimensional defects are called dislocations. They are lines along which the crystal pattern is broken. The 2-dimensional defects are surfaces, such as the external surface and the grain boundaries along which distinct crystallites are joined together. The 3-dimensional defects change the crystal pattern over a finite volume. They include precipitates, which are small volumes of different crystal structure, and also include large voids or inclusions of second-phase particles.

3.2 Point Defects

A point defect disturbs the crystal pattern at an isolated site. Points defects can be divided in to native defects (or intrinsic defects), formed only from the host atom type, and impurities (or extrinsic defects) consisting of foreign atoms. The study of defects and impurities is very crucial in the afield of semiconductors, insulators, and metal physics [48-50].Defects have profound effects on materials properties, and can be used to control their electronic and optoelectronic properties. Although they can improve some properties and turn materials into useful device components, they can also have some undesirable effects. These changes in the properties occur already for small amounts of defects, and the term dopant is usually used for an impurity atom at low concentration, which is in the order of one per million host atoms. So the desired properties can be achieved without changes in composition of the material, but just by manipulating the crystal defects. Point defects can be further divided into the following

   (i)   Vacancies
Vacancies are lattice sites which are vacant by missing atoms. In other words, a vacancy is the absence of an atom from its normal location in a perfect crystal structure.

   (ii)   Schottky defects

A Schottky defect occurs when an equal number of cations and anions are missing from their lattice sites, and the electrical neutrality of the crystal is maintained. This type of defect appears generally in ionic crystals, where the positive and negative ions do not differ too much in size. The Schottky defect is a type of vacancy named after Walter H. Schottky [51].

(iii) Interstitials

A self-interstitial is an atom from the crystal that is crowded into an interstitial site, a small void space that under ordinary circumstances is not occupied. This kind of defect is also represented in figure 3.1. In metals, a self-interstitial introduces relatively large distortions in the surrounding lattice because the atom is substantially larger than the interstitial position in which it is situated. Consequently, the formation of this defect is not highly probable, and it exists in very small concentrations, which are significantly lower than for vacancies Interstitial defects are formed when an extra atom is occupying a site in the crystal structure at which there is usually not an atom.

(iv) Frenkel defects

An atom displaced from its position to a nearby interstitial site is called a Frenkel defect, named after Yakov Frenkel.

(v) Substitutionals

Substitution defects are formed when an extra atom replaces a host atom.

(vi) Anti sites

Ant site defects are a kind of substitution defects in which a host atom occupies the site which was originally occupied by another type of host atom.

figure 3.1, schematically shows different types of defects in a crystal. Vacancies, Schottky, Frenkel, and anti site defects which do not involve foreign atoms are also called native or 'intrinsic' defects, and other defects such as interstitials and substitutionals involving foreign impurity atoms are called extrinsic' defects.
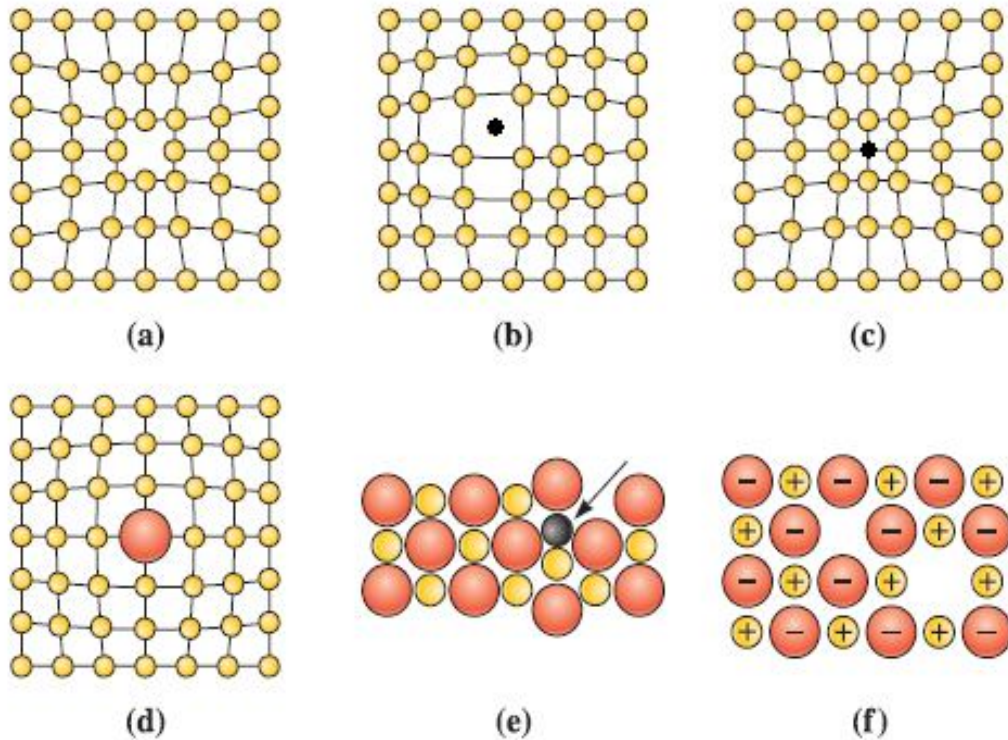
Figure 3.1: Point defects**:** (a) vacancy, (b) interstitial atom, (c) small substitutional atom, (d) large substitutional atom, (e) Frenkel defect, (f) Schottky defect

3.3 The structure of point defects

A native defect or impurity will behave differently depending on its location in the crystal lattice. An impurity can either replace a host atom at a lattice site, which is known as a substitutional impurity, or be located in an open space in-between the host atoms at an interstitial position. In III-V semiconductors there are two different substitutional sites since the impurity can either replace a group III or a group V atom. Interstitial atoms can, in principle, be located anywhere in-between lattice sites but will in practice always be located at (or close to) the most open regions where they cause the least strain on the surrounding crystal. In III-V semiconductors there are three main interstitial sites: the two tetragonal sites, either surrounded by four groups III or V atoms

and the hexagonal site. The native defects have the same types of interstitials, with the only difference being that the interstitial atom either can be a group III or group V atom. The other kinds of defects are the ant site defect, where a group III atom substitutes a group V atom at the ordinary lattice site (or vice versa) and the *vacancies*, where an atom of either type is missing from the lattice. For the impurities one can often predict whether it is going to behave like an acceptor or donor from the number of valence electrons. A group II (VI) substituting a group III (V) atom is expected to form a acceptor (donor) level in the band gap, as previously explained. For the native defects, on the other hand, it is not as apparent where their defect levels will be located in the band gap. For both vacancies and the cation anti site defect, the defect levels will ideally consist of a single non-degenerate level and a higher triply degenerate level originating from the valence band. In the neutral charge state these levels will be occupied by the electrons from the nearest-neighbors and also, in the case of the ant site, by the cations valence electrons. The lower and fully occupied $av1$-level will often remain inside the valence band and leave only the triply degenerate level in the band gap, occupied by three, five and six electrons for the anion-, cation-vacancy and cation anti site respectively. For the anion anti site and the interstitial defects, the defect levels in the band gap will instead originate from the conduction band. For the interstitials, the valence electrons of the interstitial atom will occupy a higher level and for the anion anti site the five electrons of the nearest-neighbors and the five valence electrons will first occupy the $av1$ and levels inside the valence band and the remaining two electrons will then occupy the, typically deep, level in the band gap. This rough analysis might be interesting to get a better understanding of the underlying nature of the defect levels, but the actual positions of the defect levels are, of course, very much dependent on which III-V semiconductor they are in. Even more important, the symmetry of the defect will be reduced and the degeneracy of the defect level lifted if it lowers the energy of the system (the *Jahn-Teller*

50

effect). The only way to find the magnitude of this geometrical distortion is by explicit calculation. The next section is devoted to how to calculate the defect levels in an accurate way.

3.4 Theoretical treatment of defects

For defects, either found intrinsically in or extrinsically doped into a semiconductor which is to be used in an electrical device, there are two properties of main interest: their defect levels and their concentrations. The positions and occupancies of its defect levels are of interest because it will determine if the defect act as an acceptor, deep defect or donor, as described. The defect concentration is obviously of interest because the concentration of charge carriers will be directly proportional to the concentration of the do pants. If the dopant only occurs in small numbers it will be useless no matter how good it might be in other aspects. In this section the theoretical tools for calculating there are, of course, many other properties of interest, such as the mobility and optical properties of defects and impurities, and these can be derived from that the defect levels and the defect energy (which is used to calculate the concentration). As mentioned before, defects are always present in real materials and they will therefore influence all material properties, conduction, color, magnetic behavior and so on.

3.5 Defects in alkaline-earth fluorides

Alkaline-earth fluorides occupy a special place among wide-gap dielectrics. Crystals of these compounds having the fluorite space group are widely used currently as ionizing radiation detectors, perspective elements of power optics, in scintillation equipment, etc. The use of this class of materials is impossible if their electronic structure and the formation of chemical bonds are not known in detail. A special interest presents the study of imperfect crystals, because

defects in crystals may be either a positive or negative factor for their practical applications Crystals of the fluorite group with F-centers were taken as defective crystals. These defects are model ones and have been adequately explored. With respect to theoretical methods, the interest to the study of F-centers stems from the need to describe both the defect wave function and displacements of ions surrounding a vacancy. An F-center presents interest for researcher, because it allows analyzing the relationship between electron and nuclear spins for a sufficiently large set of adjacent nuclei. Not far away the study of centers in Alkali earth fluoride has become very interesting and crucial in contemporary knowledge of defect engineering, which is aimed to tune the properties of materials in desired manner so as to get different behaviors and perfect properties.

The F center in BaF_2 is an electron localized in a fluorine vacancy and it has been identified by electron spin resonance(ESR) during Arend's investigation on addititively- colored crystal[52]. The structure is shown in figure 3.2 .Also in 1964 Arends was measured approximately the values for the peak position of the F band in CaF_2, SrF_2 and BaF_2 by investigating the effects of optical bleaching on the intensity of F-center EPR[53].In 1985 Hays& Stoneham were for the first time measured experimentally the optical absorption of the F center in CaF_2 which is found to be 3.3 eV. In the beginning of 20th century Nepomnyashchikh et al. measured that X-ray irradiation at 77 K of undoped BaF2 produces F centers having an absorption band at 2.3 eV [54].

F center in alkaline-earth fluoride crystals have had a wide range of study, this leads to find also other more complex centers, namely M and R centers composed of two and three F centers, respectively. Hayes demonstrated that F centers in additively-colored alkaline-earth fluoride crystals readily aggregate forming more complex[55],and by transmission spectroscopy Stenzel et al. showed that Al–K αX-rays generate a controllable amount of F, M, and R centers The F center in CaF_2 is an electron localized in a fluorine vacancy. The

structure is shown in figure 3.2. The electron localization function (ELF) [56] shows that the electron is well localized on the vacancy.
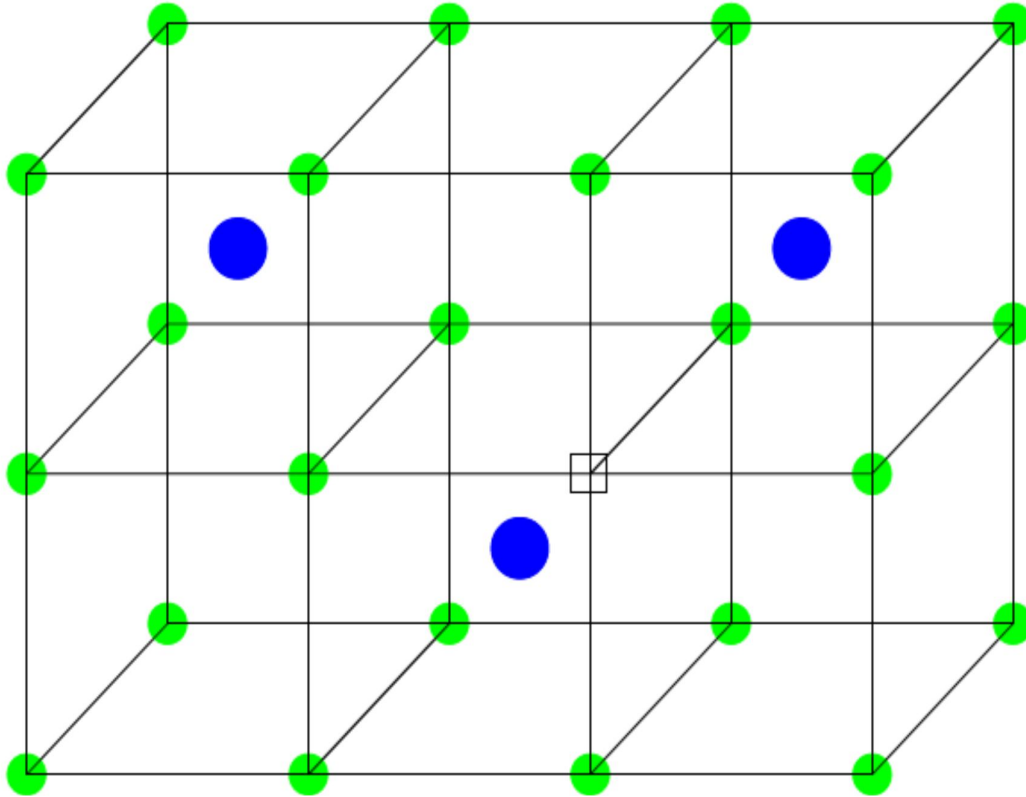
Figure 3.2: The structure of the F center: The electron is located on the fluorine vacancy (square).

3.6 Conception of the formation energy

When studying defects, the concentration of the defects is one observable which can be measured in experiments. The concentration is dependent on a number of experimental parameters, such as the concentration of impurity atoms or temperature, for example, but is also determined by the defect's formation energy, which can be calculated. The formation energy of a defect can also be determined by experiment from an Arrhenius plot of the measured concentration as a function of temperature.

The equilibrium concentration of a defect is related to its formation energy as:

$$C_D \propto e^{-(E_f(D)/K_B(T))} \tag{3.1}$$

Where C_D is the concentration of defect D, K_B and T have their usual meanings and $E_f(D)$ is the formation energy of the defect, defined as the energy required to form the defect from a source of suitable atoms. The nature of the source can vary with the defect or process being investigated and will be discussed shortly. In the neutral charge state, the formation energy is calculated as:

$$E_f(D^O) = E(D^O) - \sum_i n_i \mu_i \tag{3.2}$$

Where $E(D^O)$ is the total energy of a system containing the neutral defect, the sum is over all atomic species, n_i is the number of atoms of species i in the system and μ_i is the chemical potential of the species. The parameter μ_i is defined as the derivativeof the Gibbs free energy G with respect to n_i at constant pressure and temperature [57, 58]. G is defined as:

$$G = E + pV - TS \tag{3.3}$$

Where p and V are the pressure and volume of the system, T and S are the temperature and entropy and E is the total energy as mentioned above. The derivatives of the last two terms are negligible in most solid-state calculations, and so the chemical potential becomes:

$$\mu_i = \frac{\partial E}{\partial n_i} \tag{3.4}$$

which in turn leads to:

$$E = \sum_i n_i \mu_i \tag{3.5}$$

for a system consisting of the source of the atomic species i. A suitable source for each species will depend on the nature of the process being studied, but for the work performed in this thesis, the source of atomic host atoms (Ba,Ca or F) is taken to be a super cell of undistorted crystal.

An extra term is needed in Equation (3.2) to take into account the electron chemical potential:

$$E_f(D^q) = E(D^q) - \sum_i n_i \mu_i + q(E_V + \mu_e) \tag{3.6}$$

where q is the charge on the system, E_V is the energy of the valence band top and μ_e is the Fermi level measured from the top of the valence band. The term $(E_V + \mu_e)$ is then the calculated energy of the Fermi level, or the electron chemical potential. It should also be noted here that these equations hold true only for systems where different atoms of the same species can be considered equivalent. This is not the case for cluster calculations where host crystal atoms at different distances from the centre of the cluster will have different energies. Therefore, it is not possible to calculate formation energies in clusters, and energy comparison can be performed only between clusters containing the same number of atom in different arrangements.

3.7 Chemical Potential

As noted in the previous section, it is not straight forward to define the chemical potentials to use in Eq (3.6) for a multi-component system; in fact, it is not possible to do so uniquely, as they depend on the experimental growth conditions. However, it is possible to place from upper and lower bounds on their values independently of these conditions.

Since the chemical potential for a species represents the energy needed to add or remove one of its atoms during the formation of a defect, in order to define it we need to answer the following two questions: (i) what reservoir is the atom being removed to or taken from, and (ii) how much of the total energy of that reservoir can be attributed to this species alone. When considering one of the atomic species that constitute the host material, it is reasonable to assume that the reservoir of atoms is the material itself. Therefore, the chemical potential of a monatomic crystal is exactly equal to the energy per atom of the crystal. However, if more than one species is present, all that can be calculated is the energy per unit cell; this needs to be divided between the species. We can define

a range within which the chemical potential of each species must lie; as for the case of charged defects, therefore, all formation energies should strictly be considered to be functions of the atomic chemical potentials as well as the electronic one. Similarly as in Ref [59], applying for MF_2 (M refer to Ba or Ca) we have:

$$\mu MF_2 = \mu M + 2\mu F \tag{3.7}$$

We can place upper limits on μM and μF by noting that for MF_2 to form, Neither of these chemical potentials can be higher that the energy per atom of its species' elemental configuration. This means

$$\mu M \leq \mu M^{bulk} \tag{3.8}$$

and

$$\mu F \leq \mu F^{F^2}$$

(3.9)

where μM^{bulk} is the energy per atom of bulk M and μF^{F^2} that of an F_2 molecule. By combining these two in equalities with Eq (3.7), we can also place lower limits on the chemical potentials:

$$\mu M \geq \mu MF_2 - \mu F^{F^2}$$
(3.10)
and

$$\mu F \geq \mu MF_2 - \mu M^{bulk}$$
(3.11)

These upper and lower bounds correspond experimentally to extreme M-rich or F-rich growth conditions. Therefore it might sometimes be appropriate to simply set one of the two chemical potentials to its upper bound, depending on the experimental setup that is being considered; otherwise, the defect formation energy can be plotted as $E_f(\xi)$ for $0 \leq \xi \leq 1$ and

$$\begin{pmatrix} \mu M \ (\xi) = \mu M^{bulk} + \xi(\mu MF2 - \mu F^{F2} - \mu M^{bulk}) \\ \mu F \ (\xi) = \mu MF2 - \mu M^{bulk} + \xi(\mu F^{F2} - \mu MF2 + \mu M^{bulk}) \end{pmatrix}$$
(3.12)

We should also note that these expressions are temperature and pressure dependent while this might only have a negligible effect for bulk solids, it will certainly have a strong effect on F.

The 'richness' of one or the other component is described by the degree of non-stoichiometry of the compound. The chemical potentials depends on identifying the defect type that accommodates the deviation from stoichiometry for A-rich or B-rich conditions (and, hence, the only defect type that persists at zero temperature); this is known as the constitutional defect. For A-rich (B-rich) conditions, the constitutional defect can be either V_B (V_A) or A_B (B_A); this can be determined by comparing the sum of formation energies of several defects forming (non-interacting) stoichiometric complexes that can therefore be calculated unambiguously by atomistic simulation [60].

For impurities it is not as simple to define the reservoir; this depends on the physical provenance of the impurity atoms in the system of interest. A hard upper bound is given as before by the energy per atom of the species' elemental bulk phase. This upper bound can usually be reduced by considering the energy of other compounds that might form between the impurity and host species. However, the most direct way of estimating the chemical potential is simply to consider the experimental setup on a case-by case basis, and therefore determine the nature of the reservoir of impurity atoms; the energy per atom can then be calculated for this particular phase of the element.

3.8 Transition level

The defect transition level is defined as the Fermi energy level where two defect charge states have the same formation energies $E^f_{i(V)}$. So the transition level can be written as:

$$\mu_{i(V)}(q_1, q_2) = \frac{E^d_{i(V)}(q_2) - E^d_{i(V)}(q_1)}{q_1 - q_2}$$

(3.13)

Where, $E^d_{i(V)}(q_1)$ and $E^d_{i(V)}(q_2)$ are the defects formation energies when the Fermi level is at the valence band maximum ($E_F = 0$) ,and charge states q_1 and q_2. The calculation of the situations of the levels presented by point defects in the band gap is essential for comparison with experimental results, as these are usually what is used to identify the defect.

3.9 Image Charge Correction

The drawback of the use of standard super cell geometry is that defects are periodically and infinitely repeated spatially. The defect, instead of being surrounded by a large region of perfect bulk crystal as it would be under non-degenerate conditions, is now surrounded by mirror images of itself (figure 3.3.) This will result in somewhat frustrated ionic relaxation, though these elastic energy effects tend to be short range and is rarely a problem for even modestly -

Figure 3.3: Image charge correction schematic. The super cell (in dark green) is periodically replicated in space, due to plane wave basis, leading to artificially high defect concentrations. For charged defects this results in an overestimation of the electrostatic energy in the system. We want to correct for this to recover the 'sparse 'level of defects

Degenerate (no correction)   'Sparse' Regime (after correction)
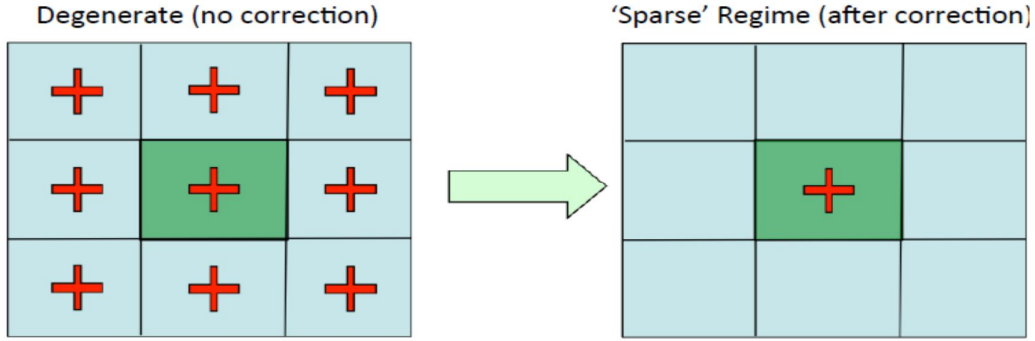
Sized cells (there is very little difference in relaxation energies for even a 2x2x2 super cell versus a unit cell of MF_2). However, when dealing with charged defects we form 'image charges' leading to spurious electrostatic interactions. These columbic interactions between the defect and its mirror charges are long-ranged and significant even for large cells. Corrections for this 'image charge' effect have been the subject of much research, though the most common approach is based on the work of Makov-Payne (MP) correction factor [61]. They considered the charge density to be the contribution of the periodic charge of the underlying crystal structure and the charge density of the periodic defect (which is simply the electron density difference between the host and host+ defect cells). The multi pole correction to the formation energy is:

$$\Delta_{MP} = \frac{q^2\alpha}{2L\varepsilon} - \frac{2\pi q Q_r}{3\varepsilon L^3} + O(L^{-5}) \tag{3.14}$$

where α is the supercell lattice-dependant Madelung constant, L is the length of the super cell, ε is the static dielectric constant, and Q_r is the second radial moment of the a periodic charge density. The first two terms are the monopole and quadrupole corrections respectively.

3.10 Potential Alignment Correction

Alkauskas et al [62, 63] .Recently made the observation that localized defect levels with respect to the average electrostatic potential are much less sensitive to computational model than with respect to the band-edges. Thus, to place the defect levels correctly with respect to the band-edges requires additional care in calculating the proper band edges relative to the electrostatic potential. It thus appears important that not only the band gap but also the individual band-edges In the case of charged defects with periodic boundary conditions there is a violation of charge neutrality, which causes the Coulomb potential to diverge[70].In momentum space formalism, one usually sets the G=0 term of the electrostatic and ionic potential (V_d (G=0) and V_I (G=0)) to zero. The Kohn-Sham eigen values are thus only defined with respect to the average electrostatic potential of the cell. For neutral systems this arbitrary offset still leads to a well-defined total energy since the electron-electron and ion-ion contributions exactly cancel. In a charged system, ignoring the G=0 term can be viewed as equivalent to a uniform background charge (jellium) compensating for the net charge - though it is important to note that this only occurs for the potential. In a charged cell there is now an arbitrary offset to the total energy. Potential-Alignment (PA) energy, which is needed for aligning the VBM between the perfect and defective super cells. PA is evaluated as:

$$\Delta_{PA} = q \ (V_d - V_p) \tag{3.15}$$

representing the difference between the average electrostatic potentials in the perfect (V_p) and defective (V_d) super cells at regions far from the defect.

CHAPTER FOUR

SIMULATIONS and DISCUSSIONS

4.1Simulations Methods

In this chapter the defect formation energy is calculated from the total energy of the bulk and defect containing simulation structures using plane-wave pseudo-potential software: Quantum Espresso[46]. We used ultra soft pseudo-potentials (USPP)[43].downloaded from Vanderbilt Ultra-Soft Pseudo-potential website [65].The calculation relies on the exchange–correlation functionality belonging to the Perdew-Burke-Ernzerhof (PBE)[18].type generalized gradient approximation (GGA). The cut-off energy for the plane wave basis set for the valence electrons is 816eV,544eV for BaF_2 andCaF_2 respectively. The defect super cells are formed by adding an interstitial atom (Ba,Ca or F) to the bulk structure or by removing an atom from it to form a vacancy. The charged defect simulation is performed by incrementing or decrementing the super cell electrons. The convergence thresholds for self- consistent calculation of the total energies were 10^{-6}, 10^{-4}, and 10^{-3} Rydberg where larger super cell has larger threshold. We employed theMonkhorst–Pack[66] mesh with $5\times5\times5,5\times5\times2$ and $2\times2\times2$ k-points to sample the first Brillouin zone in which denser mesh goes with smaller super cell. The Monkhorst-Pack grid method has been devised for obtaining accurate approximations to the electronic potential from a filled electronic band by calculating the electronic states at special sets of k points in the Brillouinzone[66]. The ground state atomic geometries were obtained by minimizing the Hellman-Feynman forces which is defined as the partial derivative of the Kohn-Sham energy with respect to the position of the ions[67,68].Since the simulation of condensed phases is concerned with a large number of electrons and a near infinite extension of wave functions, it is

necessary to use a relatively small atomistic model. The effect of edge effects on the results can be decreased by implementing periodic boundary conditions (PBC), in which a "supercell" is replicated throughout space. By creating an artificially periodic system the periodic part of the wave function is allowed to expand in a discrete set of PW's whose wave vectors are the reciprocal lattice vectors of the crystal structure. In the supercell all the atoms are relaxed from their initial positions using the Broyden-Fletcher- Goldfarb-Shanno (BFGS) [69] Hessian update method until the energy and the residual forces are converged to the limits that are set prior to running the DFT calculation. The super cells are generated from the unit cell (figure 1.1) of BaF_2, which belongs to the fluorite solid phase with cubic structure (Fm-3m space group). As shown in figure1.1, 12 atomic positions are generated by translating the base atoms, Baat (0.0, 0.0, 0.0), and F at ($0.25a$, $0.25a$, $0.25a$), with the primitive vectors ($0.5a$, $0.5a$, 0.0) , (0.0, $0.5a$, $0.5a$)and ($0.5a$, 0.0, $0.5a$); where a is the optimized lattice constant corresponding to the minimum energy of the converged total energy vs. lattice constant curve (data not shown). We use the following supercells: 2×2×2, 2×3×3 and 3×3×3 in terms of the 12 atoms unit cell (figure1.1) For example the 2×2×2, 2×3×3 and 3×3×3 super cells for bulk structure have 96, 144, and 324 atoms, respectively.The hybrid calculation is restricted to bulk CaF_2 using the less computationally demanding primitive supercell consisting of 3 atoms, Ca (0, 0, 0), F ($0.25a$, $0.25a$, $0.25a$), and F ($0.75a$, $0.75a$, $0.75a$), as indicated by the small arrows in Figure(1.1)(a). The primitive vectors in this case are (0, $0.5a$, $0.5a$), ($0.5a$, 0, $0.5a$), and ($0.5a$, $0.5a$, 0).The interstitial defect is placed in the octahedral site ($0.5a$, $0.5a$, $0.5a$) which is preferable as suggested by *Nywereet al.*[4]. All defective structures were carefully relaxed to minimize the forces between atomswith 0.08 nN as the conversion threshold on forces.

4.2 BaF$_2$ and CaF$_2$ bulk: electronic structure and calculations

Predicting the lattice constant as well as the optimal volume to a cell that has one degree of freedom is quite simple. Total energy calculations of the cell at various lattice constants around the minimal lattice constant are performed and the total energy is plotted against the volume. The minimum is found by fitting the data points to the Murnaghan equation of state [70]. Predicting the lattice parameters as well as the optimal volume for a cell that has a few degrees of freedom, such as a tetragonal or orthorhombic cell, can be done in the same fashion as one degree of freedom. However; the optimal lattice parameters need to be found self-consistently. While all but one parameter are held constant, the free parameter is simulated for a few energies around the minimum and a quadratic least squares is calculated to find the minimal value. Then the other parameters are simulated as the first. The process is repeated until the minimal parameters become self-consistent. Internal degrees of freedom are optimized for each simulation.

Since our structure is cubic and hence, has one degree of freedom we proceed by optimizing the lattice constant as described in the previous paragraph for the case of one degree of freedom. We focus on carefully optimizing the lattice constant because this optimization plays very serious role on formation energy calculations so we begin our work by calculating the lattice constant (a_o) for BaF$_2$ and CaF$_2$compare it with their experimental lattice constant as shown in Table 4.1. below which shows the calculation of a $\left(\text{Å}\right)$and the bulk modulus (B(GPa)) using various calculation methods such as the LDA and PW and PBE functionals for GGA pesudopotentials.

	Method	LDA	PW-GGA	PBE-GGA(our work)	EXP
BaF_2	a_o(Å)	6.09	6.32	6.20	6.17[71]
	B(GPa)	70.6	63	58.5	59[72]
CaF_2	a_o(Å)	5.34	5.51	5.50	5.46[72]
	B(GPa)	103[73]	83	85	82.7[73]

I have compared my data with many theoretical and experimental results as it was shown in Table 4.1. we can notice that for$BaF_2$the LDA calculations underestimates the lattice constants (a_o) by1.3% and overestimates the bulk modulus(B) by 24%.DFT with the GGAcorrection overestimates a_o by 2.4% and B by 10.5%. (PBE-GGA) gives the best result for the lattice constant a_o (overestimates only by2.2%) and also for B (overestimates by 2.6%),. For CaF_2 the LDA calculations underestimates the lattice constants (a_o) by1.3% andand overestimates the bulk modulus(B)by 24.5%.DFT with the GGAcorrection overestimates a_o by 0.9%and B by 0.4%.lastly PBE overestimates the latticeconstants(a_o) by0.7% andand overestimates the bulk modulus(B)by 2.8%.

According to the all previous results it is clear that our method(PBE-GGA) is the most consistent results with the experimental data for BaF_2 and CaF_2.

hence our calculations was in agoodaagreement with many experimental data. Figure (4.1) shows the result of our calculation of the optimal lattice constant, a_0~ 6.20Åfor BaF_2, and a_0~5.50Åfor CaF_2. The figure illustrates the total energy versus the lattice constant wherein a_0 is the lattice constant value corresponding to the minimum total energy.
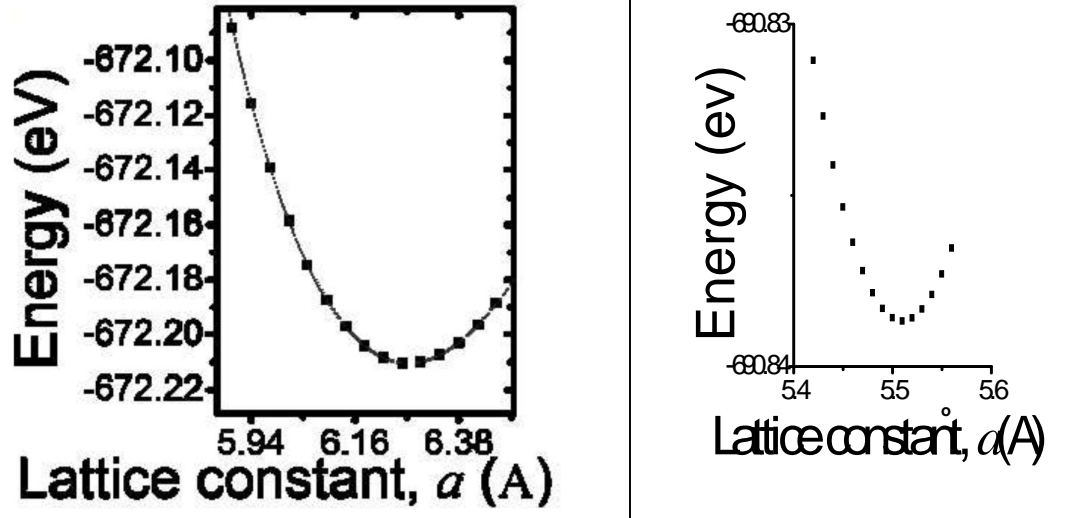
Figure4.1 (a)for BaF$_2$ The calculated (using the supercell in (a)) energy vs. the lattice constant where the optimized lattice constant ~ 6.20 Å occurs near the minimum energy. (b) for CaF$_2$ The calculated (using the supercell in (a)) energy vs. the lattice constant where the optimized lattice constant ~ 5.5 Å occurs near the minimum energy.

4.3 Simulations of BaF$_2$

4.3.1Band Gap Calculations for BaF$_2$

To determine the band gab for BaF2 we optimized value for the portion of the HartreeFock exchange energy in the hybrid functional PBE0[30]. which was found to be 28% of the exchange energy in the semilocal PBE functional. Among several portions, we find that (see figure. 4.2a) the 28% one produces a band gap, E_g^{PBE0}~ 10 eV, consistent with that obtained from mBJ method [39,40],known by its accuracy in comparison with experiment. This is clearly shown in the top panel of figure 4.2 which shows the normalised density of states (NDOS) versus the energy.Figure.4.2b shows the underestimated band gap E_g^{PBE} ~ 7 eV resulting from semilocalPBE calculation with the PW Quantum Espresso (QE) and the full potential W2k software. Again both results

correlate, especially with regard to the positions of the underestimated band-gap edges.

We stress that the PBE and PBE0 data with QE in figure 4.2. use the same norm-conserved pseudopotentials[74].On the other hand we usedultrasoft-pseudopotentialsfor the determination of the formation energies. However, the main purpose of the data in figure 4.2. is to determine the difference (i.e, correction factor) between the valence band maxima, $VBM_{PBE0} - VBM_{PBE}$, in the PBE and PBE0 calculations, which should be independent on the type of the pseudopotentials as suggested by Alkauskas*et*al[19]. Furthermore, we find it more feasible and convenient to generate the QE data in figure 4.2.using norm-conserved pseudo potentials.

VBM ~ 3.2 eV is the top of the valence band energy in bulk BaF_2 calculation. This is different from VBM_{PBE} ~ 4 eV in figure 4.2b. due to the different pseudopotentials. However, we confirm that the band gap (~7eV) is unaffected for calculations with both pseudopotentials.

The band gap reduction is a common error inherited to semilocal calculation[75]. The effect of this error on the values of the formation energies will be corrected through the correction factor $VBM_{PBE0} - VBM_{PBE}$ ~ 2 eV figure.4.2. Another source of error emanates from the interaction between the periodic charge images that can be corrected as discussed in Ref [76].This error is significant for small supercells and has, thus, not been considered in our calculations which use larger supercells.
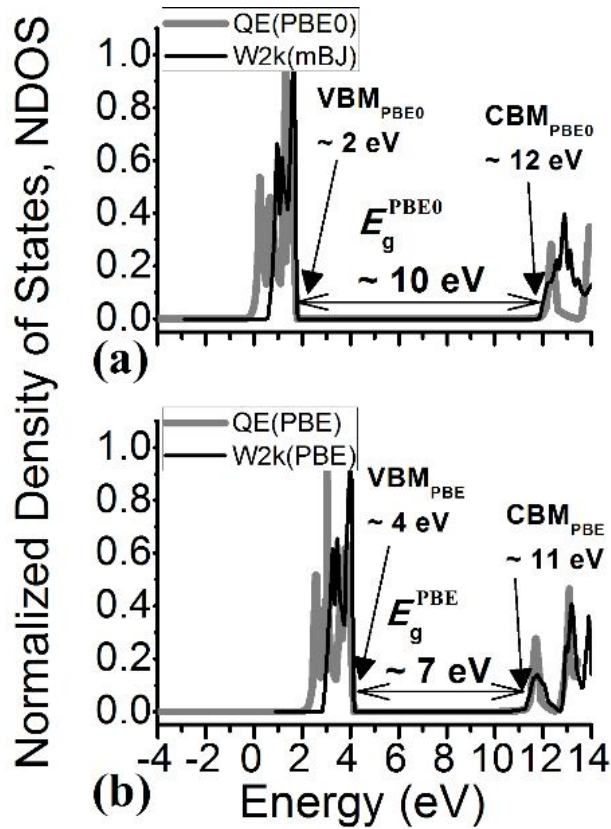
Figure 4.2 The normalized density of states (NDOS) calculated with (a) hybrid GGA type PBE0 (thick grey line) using QE software and with mBJ corrected GGA (black line) implemented in W2k software (b) GGA type PBE (thick grey line) using QE software and with GGA type PBE (black line) using W2k software . The energy values for the Valence Band Maxima (VBM) and Conduction Band Minima (CBM) are indicated for each type of calculations by solid arrows.

4.3.2 BaF$_2$ Formation Energy with Extrapolation Technique

Recently, Nyawere*et al.*[4].pointed out that measured formation energy of native defects in BaF$_2$ is limited to anion defects. They also pointed out the fact that there is a shortage in the theoretical calculation of the defect formation energy in BaF$_2$. However, they focused on ab-initio calculations for the identification of stable native defects in BaF$_2$ using small supercell with 96 atomic sites. Therefore, in this thesis we built upon their work by extending the

simulation supercell up to 325 atoms, focusing on the calculation of the charge transition levels for native vacancies and interstitials. The values of the levels are extrapolated to the limit of infinite supercell size.

The formation energies E_i^f and E_V^f, respectively, for interstitial and vacancy are:

$$E_i^f = E_i^q - E_b - \varepsilon + q\ (E_F + \text{VBM}) \qquad (4.1)$$
$$E_V^f = E_V^q - E_b + \varepsilon + q\ (E_F + \text{VBM}) \qquad (4.2)$$

Where, $E_{i(V)}^q$ is the relaxed total energy of the charged (with charge q) defect structure, E_b is the calculated total energy of bulk supercell, E_F is the electrons Fermi energy, and ε is the defect chemical potential approximately taken as the simulationenergy of a single defect in a large empty cubic cell (12 Å side). We obtained ε = -70.14 Ry and -48.34 Ry for free Ba and F, respectively. VBM ~ 3.2 eV is the top of the valence band energy in bulk BaF_2 calculation. This is different from VBM_{PBE} ~ 4 eV in Figure (4.2).(b) due to the different pseudopotentials. However, we confirm that the band gap (~ 7 eV) is unaffected for calculations with both pseudopotentials.

Table.4.1. compares the formation energies from this work with those calculated by Nywere*et al*[4] using the smallest 2×2×2 supercell at E_F = 0. Obviously both data are in close agreement. Figure 4.3: shows $E_{i(V)}^f$ (at E_F= 0) versus the reciprocal of the supercell size (L= the cubic root of the supercell volume) for charged F^{-1} and Ba^{+2} interstitials and vacancies. The linear trend of the data stimulates the linear extrapolation (solid lines, figure 4.3.) of $E_{i(V)}^f$ to the limit L^{-1} = 0 corresponding to infinitely large supercell. The extrapolation method allows for the estimation of values at a limit of very large.
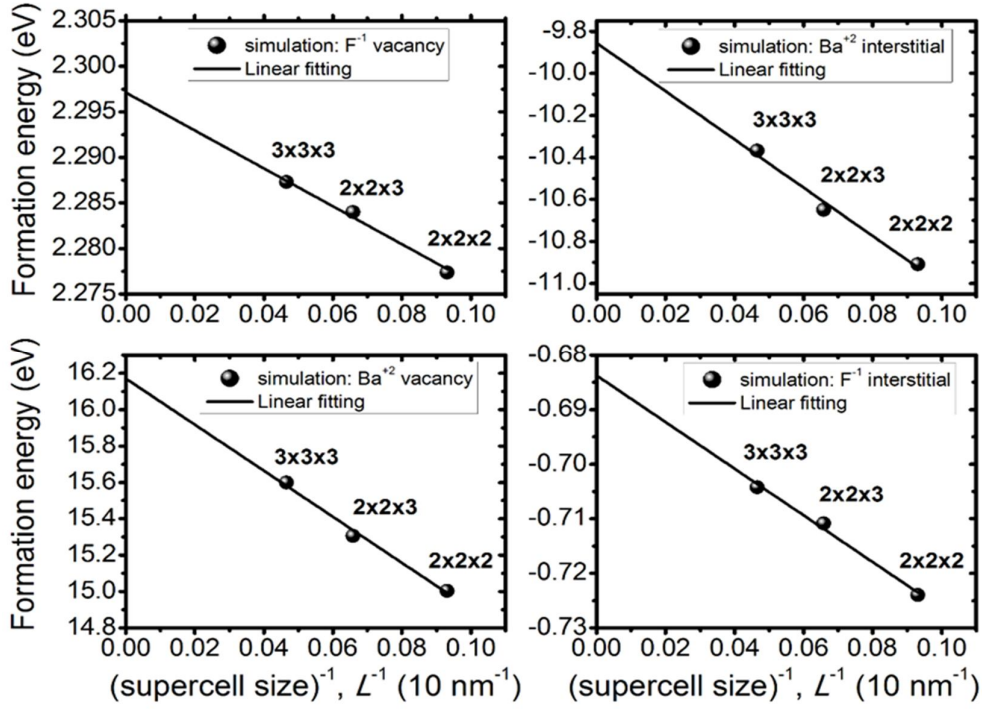
Figure 4.3: The calculated formation energy vs. inverse supercell size (L^{-1}) for charged F^{-1} and Ba^{+2} interstitials and vacancies in BaF_2 structure. The simulation supercells are $2\times2\times2$, $2\times2\times3$ and $3\times3\times3$ in terms of a 12 atoms unit cell (figure 1.1). The vacancy- (interstitial-) supercell has one atom less (extra atom). supercells that are computationally intractable[76]. The values of $E_{i(V)}^{f}$ at $L^{-1} = 0$ are listed in the last column in Table 4.2.

Table 4.2 :The formation energy (at $E_F = 0$) for native defects in BaF_2.

Defect	Formation energy (eV)		
	Our calculation ($2\times2\times2$) cell	Nywere*et al* [4] ($2\times2\times2$) cell	Extrapolated to $L^{-1} = 0$ (Figure.4.3)
Ba^{+2} interstitial	-10.91	-11.25	-9.82
Ba^{-2} vacancy	15.01	15	16.20
Ba^0 interstitial	3.34	3.14	3.69
Ba^0 vacancy	15.51	15.64	15.67
F^0 interstitial	-0.97	-0.62	-0.82
F^0 vacancy	9.27	8.73	9.68
F^{-1} interstitial	-0.72	-0.69	-0.68
F^{+1} vacancy	2.28	2.29	2.30

According to Shi *et al*[14]the formation energy for the F^0 vacancy is 7.82 eV which is lower than our extrapolated one by ~ 1.8 eV. This could be due to the different atomic potential used in their work and to their employment of smaller supercells than ours. However, we believe that our extrapolated data are more reliable owing to increased accuracy associated with large supercell calculations.

In concurrence with Ref.[1], we found that the octahedral site is favored, and accordingly, all counts reported beneath allude to the interstitial in the octahedral site. The estimations of the formation energies are appeared in Table 4.2. The more negative the vitality, the less demanding it is to frame such a deformity. Thus, the formation of neutral flourine interstitial is easier than the barium interstitial.

We are now going to discuss about the existence of stable native defects in BaF_2 structures. It is important to point out that the formation energies used are those extrapolated to the limit of infinite supercell size as listed in the last column of Table 4.2. This will render our estimation of the formation energies and the transition levels (to be discussed afterwards) more accurate than Amolo et al calculations.
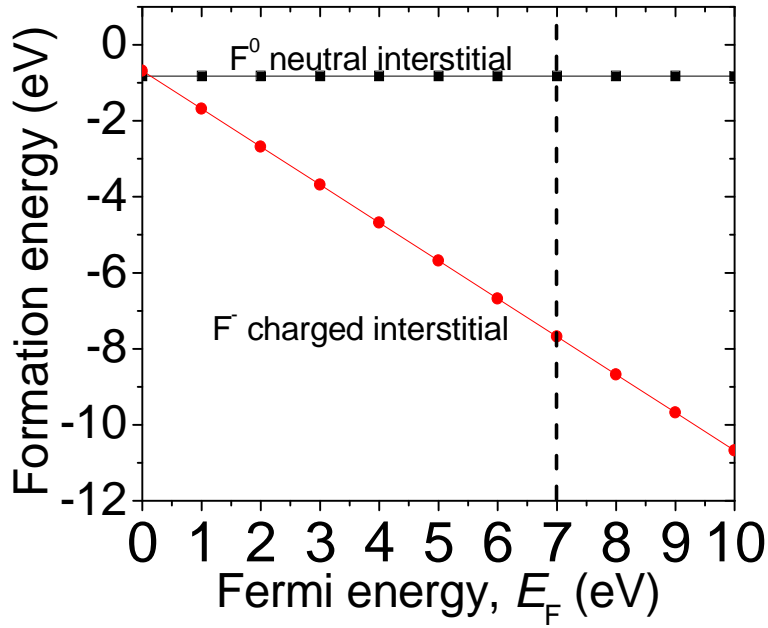
Figure 4.4:(Color online) Formation energy as a function of Fermi energy for F and F$^-$ interstitial defects in BaF$_2$.
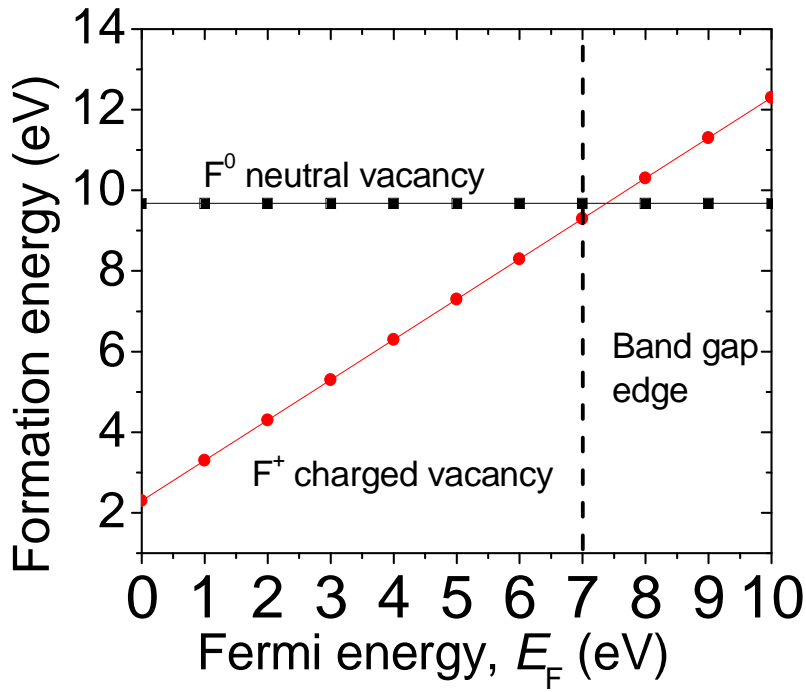
Figure 4.5:(Color online) Vacancy formation energies as a function of Fermi energy for F and F$^+$

Figure 4.4.illustrates the interstitial formation energies for F and F⁻ versus the Fermi level. On account of neutral F the line is parallel to the E_F axis and crosses the formation energy axis at -0.82 eV. However, F⁻ has formation energies less than that for the neutral F, indicating that F⁻ is more stable than the neutral F. We in this manner infer that the anion interstitial in BaF$_2$ is contrarily charged. figure 4.5:shows the formation energies versus E_F for vacancies formed by removing F and F⁻. The formation energy of the neutral vacancy is 9.68 eV. In an extensive scope of estimations of the E_F (up to around 6 eV), we find that the charged vacancy of F⁻, which is positively charged, is more stable than the neutral F. Therefore since the band gap ~7 eV, we infer that the fluorine vacancy is positively charged except for the cases when E_F is greater than the conduction band, i.e. when the structure is heavily doped with donors.
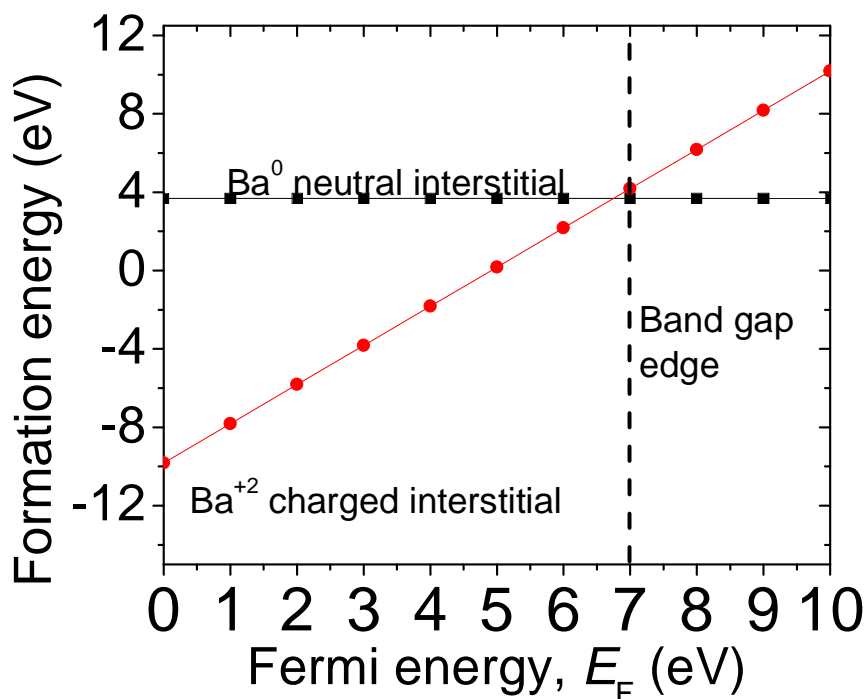
Figure 4.6:(Color online) Interstitial formation energies as a function of Fermi energy for Ba and Ba^{+2}
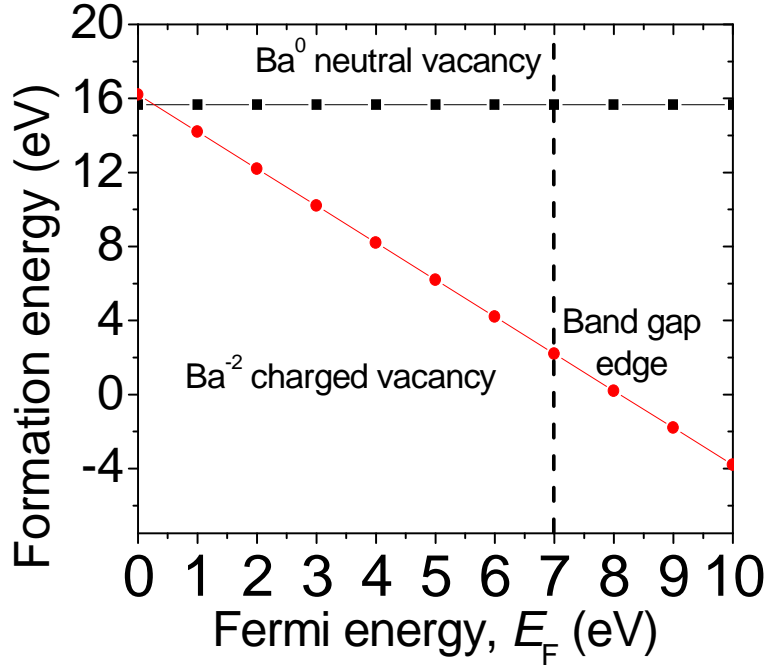
Figure 4.7:(Color online) Ba vacancy formation energy as a function of Fermi energy for Ba and Ba^{-2}

Figure .4.6.and figure .4.7. demonstrate the formation energies versus E_F for Ba interstitial and vacancy. Clearly the curve for neutral Ba interstitial intersects with the vertical axis at the formation energy of 3.69 eV. However the formation energies for the charged Ba interstitial is smaller than that for the neutral counterpart for all E_F within the band gap. Therefore the charged Ba interstitial is expected to be more stable than the neutral one. For the Ba vacancies figure.4.7, it is clear that the formation energies for the charged one are smaller than the neutral one for all E_F within the band gap.

Frenkel defects are defined to be formed by shifting the atom from it substitutional position to an interstitial position, producing a vacancy-interstitial pair. Assuming that the pairs are weakly interacting (for example sitting far apart), their formation energy can be regarded as the summation of the formation energies of the isolated interstitial figure 4.4. and vacancy figure 4.5 .Therefore, it is possible to regard the fluorine Frenkel defects as always consisting of charged defects. This is true only when E_F is in proximity to the

conduction band minimum where we have charged interstitial but neutral vacancy. In the case that both defects are charged then the formation energy of the F Frenkel defect is 1.62 eV for all E_F till near the bottom of the conduction band. This is completely opposite to the finding of Amolo et al who reported a range of formation energy from 2.33 to -0.8 eV near the conduction band. Their error arises from uncorrected calculation of the formation energy. While in our case the calculation has been corrected with the extrapolation method as discussed above. From figuers. 4.6 and 4.7, it is clear that the Barium Frenkel defects consist of charged defects for all E_F with formation energy ~ 3.90 eV.

4.4 The transition level calculations and corrections methods

4.4.1 BaF$_2$ transition level

The defect transition level is defined as the Fermi energy level where two defect charge states have the same $E_{i(V)}^f$ as it was in Equations (3.13) so the values of $E_{i(V)}^d(q)$ are listed in the last column of Table 4.2 for charged (with charges +2, -2, +1, and -1) and neutral (0 charge) defects. The values of $\mu_{i(V)}(q_1, q_2) \equiv \mu_{\text{semilocal}}$ are shown in the first column of Table 4.3 where (0, -2), (+2, 0), (+1, 0), and (0, -1) are the charge transitions (q_1, q_2) for, respectively, Ba vacancy (Ba$_v$), Ba interstitial (Ba$_i$), F vacancy (F$_v$), and F interstitial (F$_i$). $\mu_{\text{semilocal}}$ are the values before the correction for the error arising from the band gap underestimation. The correction factor $\delta = \text{VBM}_{\text{PBE0}} - \text{VBM}_{\text{PBE}} \sim 2$ eV (figure 4.2) can be added to $\mu_{\text{semilocal}}$ to place the level in the corrected band gap, $E_g^{\text{PBE0}} \sim 10$ eV (see figure 4.2a), associated with the PBE0 calculation. The corrected values $\mu_{\text{corrected}} = \mu_{\text{semilocal}} + \delta$ are listed in the second column of Table 4. 2. It is clear that $\mu_{\text{corrected}}$ are given with reference to the VBM$_{\text{PBE0}}$ and, hence, falling within the corrected band gap E_g^{PBE0} (figure 4.2b). On the other hand $\mu_{\text{semilocal}}$ are given with respect to VBM$_{\text{PBE}}$ (figure 4.2a).

The above procedure of correcting the level positions follows tightly the correction recipe suggested in Ref [19]. The condition for implementing this recipe is that VBM_{PBE0} and VBM_{PBE} (figure 4.2) must be given with reference to a common ionic electrostatic potential. Satisfying this condition leads to the alignment of $\mu_{corrected}$ and $\mu_{semilocal}$ as demonstrated in Ref [19]. Such condition is true in our case since the QE calculations in figure 4.2 are based on the same pseudopotentials. Additionally the default energy scale in QE software is set relative to the ionic electrostatic potential. In other words the energy scale in figure 4.2 for the QE data is automatically given with respect to the ionic electrostatic potential. That is why the W2k NDOS figure 4.2 are manually shifted to align with that from QE calculation since the main purpose of the W2k data is to optimize the band gap size.

Table 4.3: The correction of the transition levels ($\mu_{semilocal}$) from semilocal calculation using the correction factor $\delta = VBM_{PBE0} - VBM_{PBE} \sim 2$ eV in figure 4.2. $\mu_{semilocal}$ is given with respect to VBM_{PBE0}.

Defect	Charge transition	$\mu_{semilocal}$ (eV)	$\mu_{corrected}$ (eV) = $\mu_{semilocal} + \delta$
Ba_v	(0, -2)	0.27	2.27
Ba_i	(+2, 0)	6.76	8.76
F_v	(+1, 0)	7.38	9.38
F_i	(0, − 1)	0.14	2.14

Figure 4.10a shows the positions of $\mu_{semilocal}$ in the plane of the formation energy versus the E_F. These levels occur at the crossings of the dotted lines representing equations (4.1) and (4.2) with slopes q (0, $\pm$ 1 and $\pm$ 2) and intersecting the vertical axis at the extrapolated values (Table 4.2) of the formation energies. Clearly the semilocal calculation predicts the occurrence of $F_v^{+/0}$ within the conduction band, which is the case if the material is degenerately doped with donors. However, in contrast to semilocal result, the

corrected $F_v^{+/0}$ level in Table 4.2 is predicted to be ~ 0.6 eV below the CBM$_{PBE0}$. Generally, the hybrid-semilocal calculations predict that the levels ($\mu_{corrected}$, Table 4. 1) are located within the band gap with minimum separation ~ 0.6 eV (for $F_v^{+/0}$) from the corrected CBM$_{PBE0}$ (figure 4.2), while the uncorrected semilocallevels $\mu_{semilocal}$ are almost touching with the underestimated band edges (VBM$_{PBE}$ and CBM$_{PBE}$, figure 4.2).

We will now assess the validity and accuracy of the extrapolated formation energies in Table 4.2. The necessity of this assessment is evident since the accuracy of extrapolation process is a key factor for the accuracy of the transition levels. For this purpose we will apply specific set of correction schemes to calculate the defect formation energies using relatively small supercells, 2×2×2 and 1×2×3. An agreement between the corrected and extrapolated energies will then signify the validity of the extrapolation method. For example, in figure.7 of Lany*et* al[83] the corrected formation energies from supercells with ≥ 64 atoms agree with the extrapolated ones.

4.4.2 Makove Payne and Potential Alingment calculations

The formation energies from supercell calculation can be corrected to eliminate the small supercell size effects such as the unwanted interaction energy between image charges in periodic supercells, which is accounted for by incorporating the Makov-Payne (MP) correction factor in Eq (3.14)in chapter 3by taking the momople term,so the equations can be written as follow:

$$\Delta_{MP} = \frac{q^2 \alpha}{2L\varepsilon} \tag{4.3}$$

where$\varepsilon = 7.33$ is the dielectric constant for BaF$_2$, $\alpha = 2.83$ is the Madelung constant for our cubic structure, q is the charge state of the defect, and $L=$

11.266 Å (1×2×3 cell) and 12.8Å (2×2×2 cell) is the cubic root of the supercell volume. Δ_{MP} represents the first term in the MP factor, which will lead to sufficient accuracy in the corrected formation energies as will be discussed in conjunction with Table 4.4.

Another correction factor is the Potential-Alignment (PA) energy, which is needed for aligning the VBM between the perfect and defective supercells. PA is evaluated as $\Delta_{PA} = q (V_d - V_p)$, representing the difference between the average electrostatic potentials in the perfect (V_p) and defective (V_d) supercells at regions far from the defect. This is performed using the post-processing module (namely the code pp.x) in the QE software to evaluate the spherical average of the potential far from the defect.

Incorporating the above factors in equations (4.1) and (4.2) yields the following equations (4.4) and (4.5) to be used for the evaluation of the corrected formation energies:

$$E^f_{i,corr} = E^f_i + \Delta_{MP,i} + \Delta_{PA,i} \tag{4.4}$$

$$E^f_{v,corr} = E^f_v + \Delta_{MP,v} + \Delta_{PA,v} \tag{4.5}$$

Where Δ_{MP} and Δ_{PA} is the estimated factors along with the values of E^f_{corr} at $E_F = 0$ calculated using 2×2×2 and 1×2×3 supercells.

Figures 4.8 and 4.9, illustrates the good and accurate potentials alignment for2×2×2 and 1×2×3 supercells
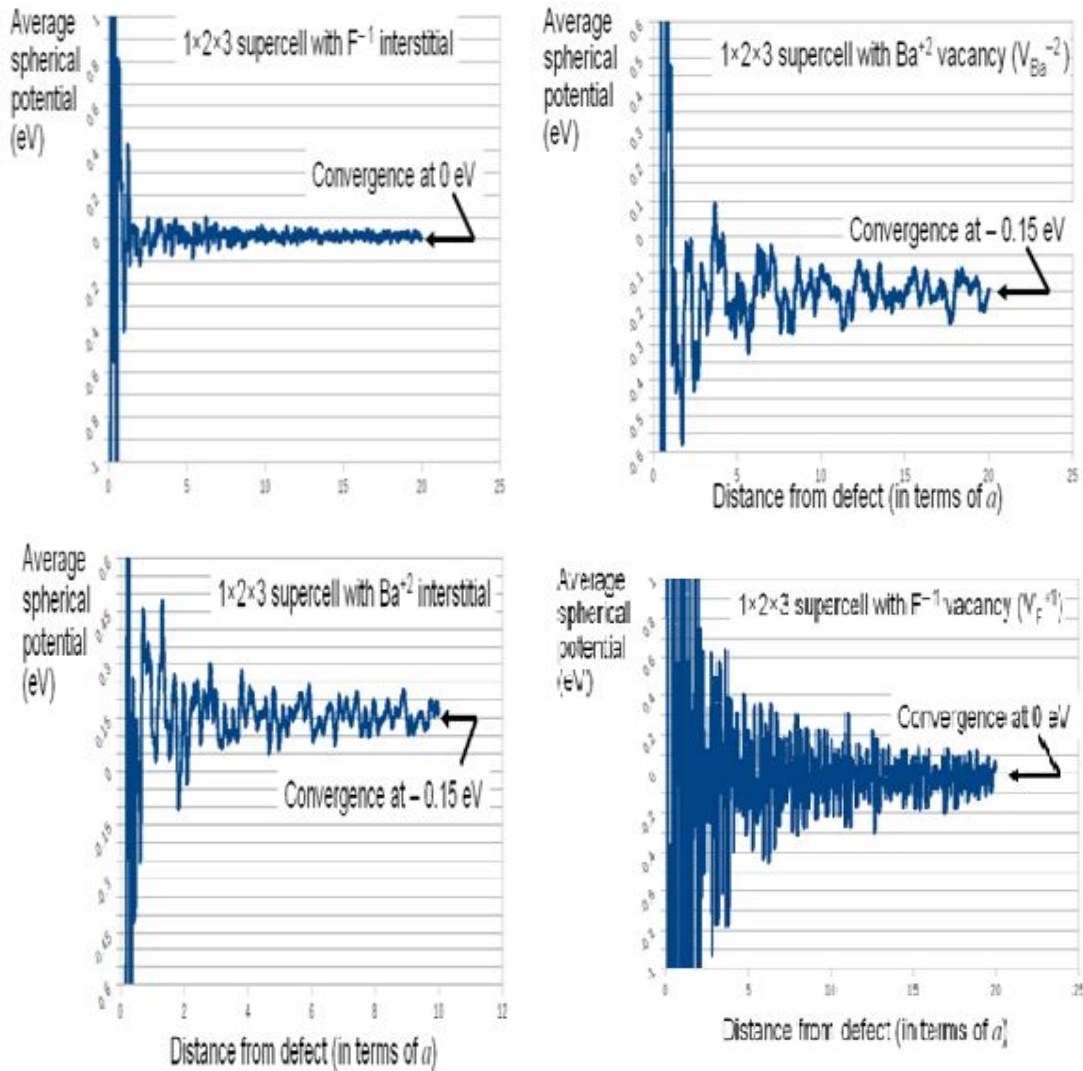
Figure 4.8: The potentials alignment for 1×2×3 super cell with Ba,F interstitials and vacancies.
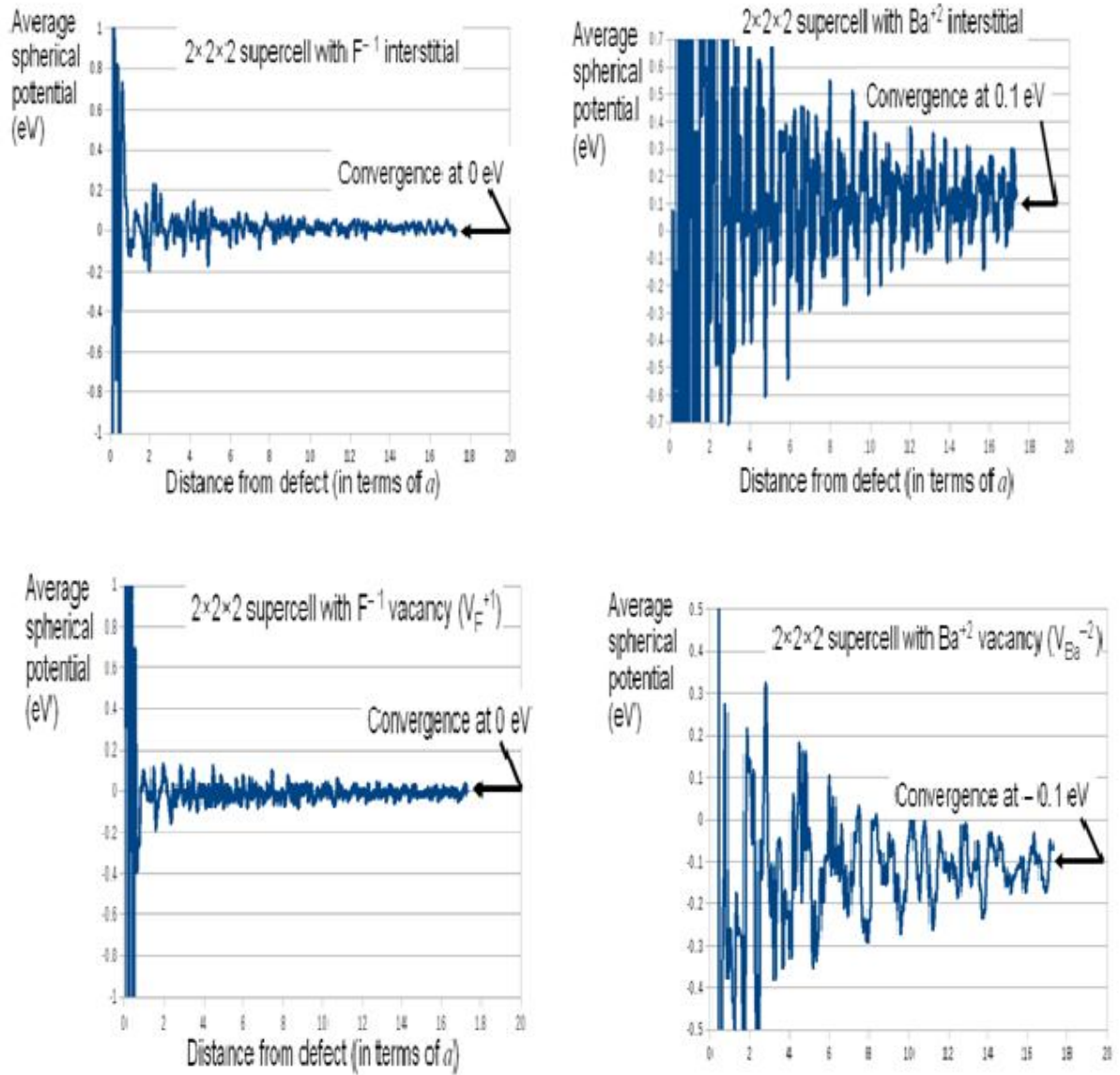
Figure 4.9: The potentials alignment for 2×2×2 super cell with Ba,F interstitials and vacancies.

Table 4.4: shows the estimated factors Δ_{MP} and Δ_{PA} along with the values of E^f_{corr} at $E_F = 0$ calculated using 2×2×2 and 1×2×3 supercells. It is evident that the corrected E^f_{corr} obtained by using small supercells are consistent with each other and with the extrapolated values in Table 4.2. This consistency between

the corrected and extrapolated formation energies indicates that the extrapolated data are reliable.

Table 4.4: The corrected formation energies obtained with 2×2×2 and 1×2×3 supercell calculation using Makov-Payne (MP) and Potential-Alignment (PA) correction methods

Defects	Charge state	Δ_{MP} (eV)		Δ_{PA} (eV)		E^f_{corr} (eV)	
		2×2×2	1×2×3	2×2×2	1×2×3	2×2×2	1×2×3
Ba_i	+2	0.899	0.990	0.10	0.15	− 9.911	− 9.283
Ba_v	− 2	0.899	0.990	− 0.10	− 0.15	15.809	16.414
F_i	− 1	0.225	0.247	0.00	0.00	− 0.495	− 0.630
F_v	+1	0.225	0.247	0.00	0.00	2.505	2.485

For simplicity we have not considered the band-filling effect, discussed in Ref[3], which usually emerges for structures with high impurity concentration, leading to the formation of band-gap impurity bands. figure 4.10b shows our calculated DOS vs. energy in defective 3×3×3 supercells. The data illustrates the presence of very sharp band gap peaks such as the one indicated as "$Ba_i d$-level' arises from the d-orbitals of the interstitial Ba^{+2} defects as revealed from the projected DOS calculations (using the projwfc.x code in QE). Thus, the data in figure 4.10b show no clear formation of broad and delocalised impurity band in the band gap, suggesting that we are working in the dilute limit regime of the defect concentration which may minimize the band-filling effect. Here it is worth mentioning that the sharpness of the band gap DOS indicate that the defect wave functions are localized. The localization of the defect wavefunctions is required [19] for better accuracy in the calculation of the transition levels using the hybrid and semilocal scheme employed in this work. Additionally, this scheme works better for wide band gap materials as clearly illustrated in figure 4.2a in Ref[19]. Indeed our BaF_2 with wide band gap satisfies this requirement as well.
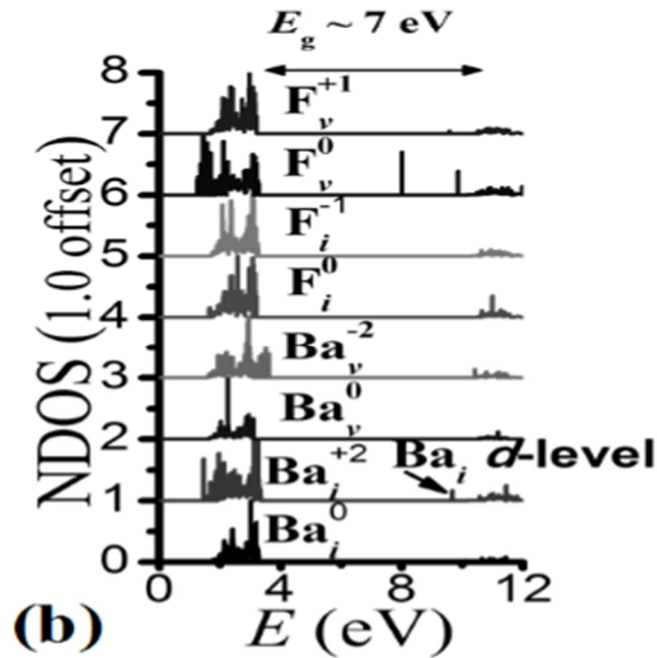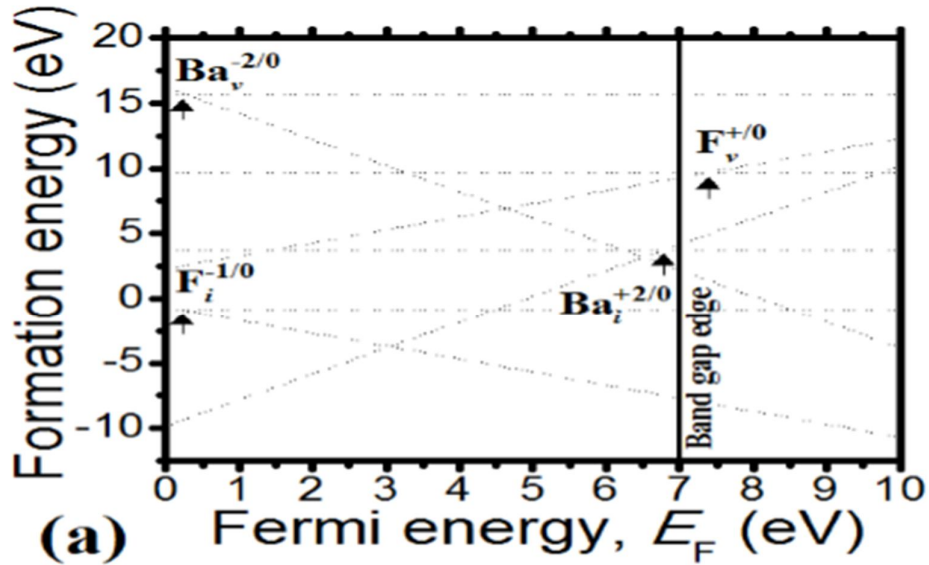
Figure 4.10a: The semilocal transition levels, $\mu_{\text{semilocal}}$, from Table 4.3 are indicated by small arrows in the plane of the formation energy (E_f) versus E_F. The dashed thin lines correspond to equations (4.1) and (4.2) with slope q and intersections represented by the extrapolated E_f in Table 4.1b. The calculated normalized density of states using 3×3×3 defective supercells. The PBE band gap is $E_g \sim 7$ eV.

Finally we comment on that the formation energies for Ba_i^{-1} and Ba_i^{+1} interstitials from semilocal calculations on 2×2×2 supercells have been found to be -14.1 eV and -20.5 eV. These indicate the high stability of these defects in the structures. However, they require careful adjustment of the simulation parameters for convenient convergence of the results. We will thus also consider the analysis of these defects in future work.

4.5 The simulations of CaF_2

4.5.1 Band gab calculations of CaF_2

In this section we focus on the first principle calculation of the charge transition levels for native vacancies and interstitials in CaF_2. The charge transition level is defined as the Fermi energy where two defect charge states have the same formation energy. We use the plane-wave (PW) density functional (DFT) method with the semilocal generalized-gradient-approximation (GGA) [5] pseudo-potentials known to underestimate the band gap. In order to locate the transition levels within the corrected band gap, we followed a similar approach as described in Ref[19] where the correction of the band gap is achieved by using hybrid PBE0 functional in GGA calculation. Our band gap from PBE0 calculation is ~ 10.6 eV, which correlates well with the experimental gap ~ 12 eV[1]. Thus the position of the transition levels are referenced to the corrected valence band maximum (VBM_{PBE0}) in the PBE0 calculation.

Finally we validated the band gap calculations using the Tran-Blaha modified-Becke-Johnson (TB mBJ[39]) correction to GGA employed by the DFT Wien2k[40] (here after referred to as w2k) simulation package which is a full-potential code based on Linearized Augmented Planewave (LAPW) method, known for its accuracy. The calculated band gap from mBJ calculation was ~ 10.6 eV, matching well with that from the PBE0 calculation.

The optimized value for the portion of the HartreeFock exchange energy in the hybrid functional PBE0[30] is 25% of the exchange energy in the semilocal PBE functional. As illustrated in figure 4.2b (Normalized Density of States (NDOS) versus the energy) we find that the 25 % one produces a band gap, E_g^{PBE0} ~ 10.6 eV, consistent with that obtained from mBJ method[39,40] known by its accuracy in comparison with experiment. Figure 4.11a. shows the underestimated band gap E_g^{PBE} ~ 8.3 eV resulting from semilocal PBE calculation with the PW Quantum Espresso (QE) and the full potential w2k software. Again both results correlate, especially with regard to the positions of the underestimated band-gap edges.

We stress that the PBE and PBE0 data with QE in figure 4.11 use the same norm-conserved pseudo potentials[74]. On the other hand we used ultrasoft-pseudopotentials[43] for the determination of the formation energies. However, the main purpose of the data in figure 4.11 is to determine the difference (i.e, correction factor) between the valence band maxima, $\text{VBM}_{\text{PBE0}} - \text{VBM}_{\text{PBE}}$, in the PBE and PBE0 calculations, which should be independent on the type of the pseudopotentials as suggested by Alkauskas*et al*[19]. Furthermore, we find it more feasible and convenient to generate the QE data in figure 4.11 using norm-conserved pseudo potentials.
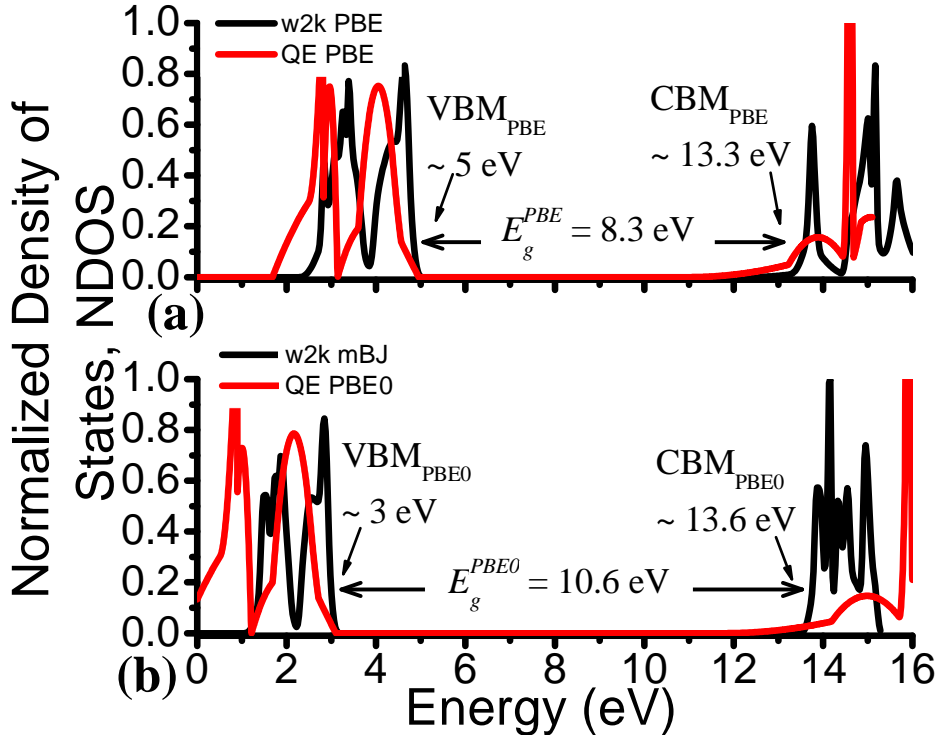
Figure.4.11: The normalized density of states (NDOS) calculated with (a) GGA type PBE (red line) using QE software and with GGA type PBE (black line) using w2k software. The energy values for the Valence Band Maxima (VBM) and Conduction Band Minima (CBM) are indicated for each type of calculations by solid arrows. (b) Hybrid GGA type PBE0 (red line) using QE software and with mBJ corrected GGA (black line) implemented in w2k software.

4.5.2 Formations energies with Makove Payne corrections

As it was in equations (4.1) and (4.2) :

ε is the defect chemical potential approximately taken as the simulation energy of a single defect in a large empty cubic cell (12 Å side). We obtained ε = -74.78 Ry and -48.32 Ry for free Ca and F, respectively. VBM ~ 3.4 eV is the top of the valence band energy in bulk CaF_2 calculation. This is different from VBM_{PBE} ~ 5 eV in figure 4.12a due to the different pseudopotentials. However,

we confirm that the band gap (~ 8.3 eV) is unaffected for calculations with both pseudopotentials.The band gap reduction is a common error inherited to semilocal calculation[75]. The effect of this error on the values of the formation energies will be corrected through the correction factor $VBM_{PBE0} - VBM_{PBE} \sim 2$ eV (figure 4.11b). Another source of error in the value of the formation energy emanates from the interaction between the periodic charge images that can be corrected through the employment of the Makov-Payne (MP) correction factor[76].

Table 4.5.shows the calculated values of the corrected ($E_{f,corr} = E_f + \Delta_{MP}$) and uncorrected ($E_f$) formation energies using equations (4.1)-(4.2) , $2\times2\times2$ and $3\times3\times3$ supercells at $E_F = 0$, where the Makov-Payne correction factor $\Delta_{MP} \approx q^2 \alpha/(2\kappa L)$. Here, $\kappa = 6.81$ is the dielectric constant for CaF_2, $\alpha = 2.83$ is the Madelung constant for our cubic structure, q is the charge state of the defect, and $L = 5.5$ Å ($2\times2\times2$ cell) and 16.5 Å ($3\times3\times3$ cell) are the cubic root of the supercell volumes. Δ_{MP} represents the first term in the MP factor, which will lead to sufficient accuracy. Obviously values of $E_{f,corr}$ from both $3\times3\times3$ and $2\times2\times2$ calculations are in excellent agreement with each other. Therefore, the average formation energies, $E_{f,avg}$, from both supercells are listed in the column of Table 4.5 .We point out that, for the large $3\times3\times3$ supercell, we limit the calculation to the charged defects. Also for simplicity we ignore the potential alignment[83] correction energy for the defects.

Table 4.5: The corrected, $E_{f,corr}$, (using Makov-Payne factor, Δ_{MP}) and uncorrected, E_f, formation energies at $E_F = 0$ for native defects in CaF_2. The calculations are performed for $2\times2\times2$ and $3\times3\times3$ supercells.

Defect	E_f (eV)		Δ_{MP} (eV)		$E_{f,corr} = E_f + \Delta_{MP}$		$E_{f,avg}$ (eV)
	$2\times2\times2$	$3\times3\times3$	$2\times2\times2$	$3\times3\times3$	$2\times2\times2$	$3\times3\times3$	
Ca^{+2} interstitial	-11.30	-10.31	1.09	0.73	-10.21	-9.58	-9.895
Ca^{-2} vacancy	15.37	15.97	1.09	0.73	16.46	16.7	16.58
F^{-1} interstitial	-0.54	-0.41	0.28	0.18	-0.26	-0.23	-0.245
F^{+1} vacancy	2.31	3.00	0.28	0.18	2.59	3.18	2.885
Ca^0 interstitial	3.40	--	0	--	3.40	--	3.4
Ca^0 vacancy	15.78	--	0	--	15.78	--	15.78
F^0 interstitial	-0.54	--	0	--	-0.54	--	-0.54
F^0 vacancy	8.71	--	0	--	8.71	--	8.71
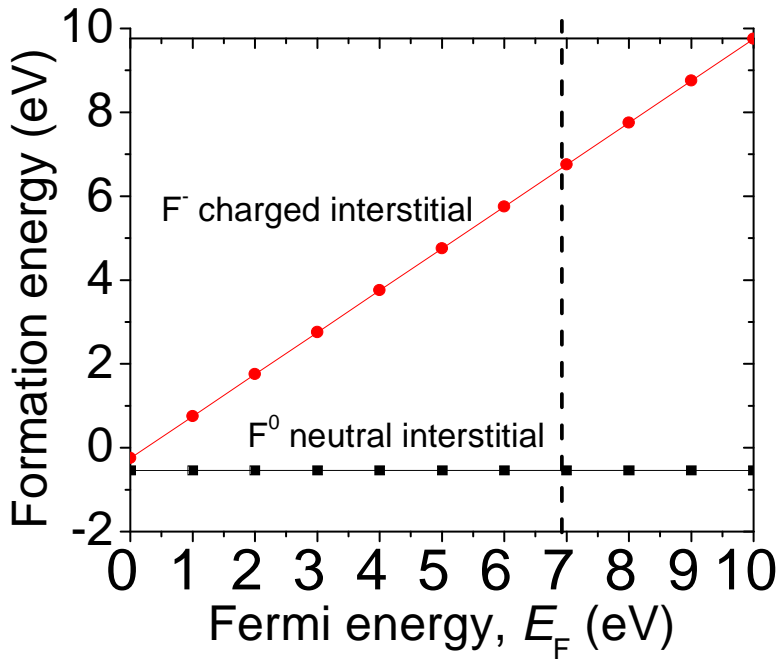
Figure 4.12:(Color online) Formation energy as a function of Fermi energy for F and F⁻ interstitial defects in CaF_2.
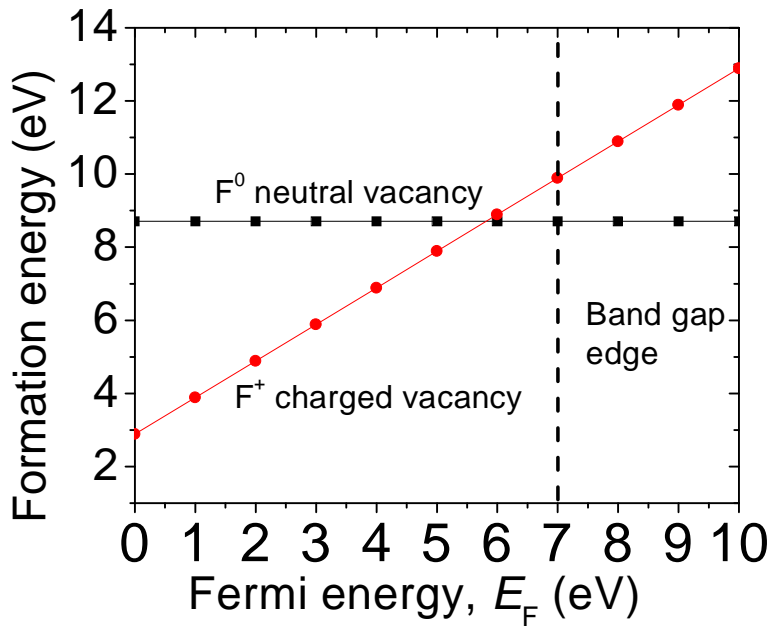
Figure 4.13:(Color online) Vacancy formation energies as a function of Fermi energy for F and F⁺ in CaF_2
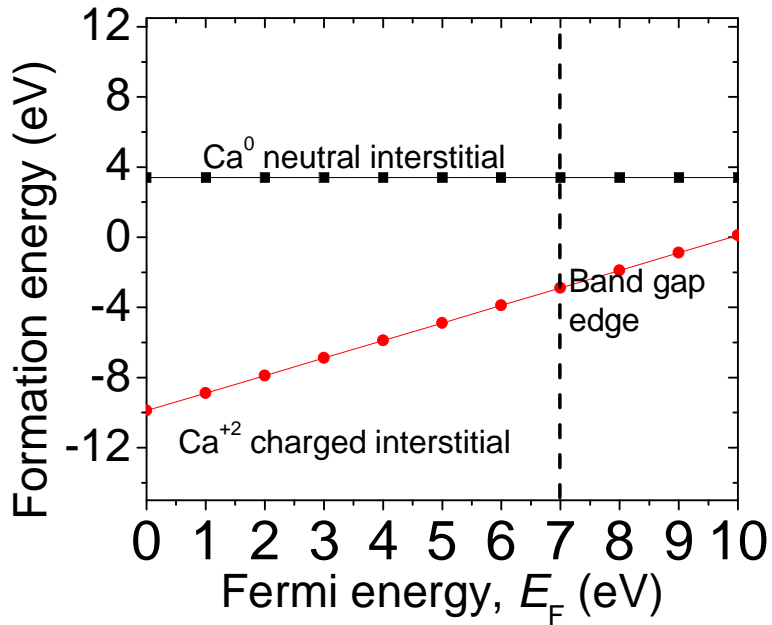
Figure 4.14: (Color online) Interstitial formation energies as a function of Fermi energy for Ca and Ca^{+2}
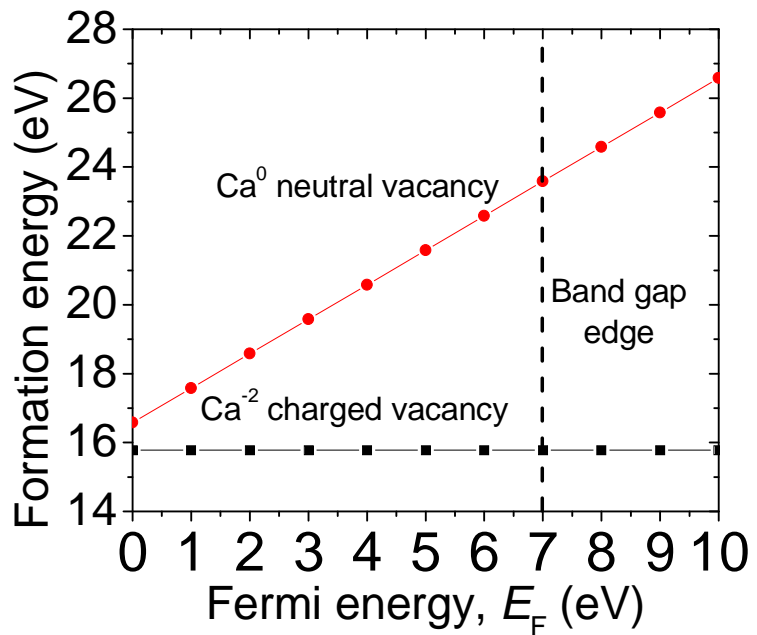
Figure 4.15: (Color online) vacancy formation energies as a function of Fermi energy for Ca and Ca^{+2}

4.5.3 The corrected Transition level calculations for CaF$_2$

We calculated the transiton level for CaF$_2$ from Equations (4.1),(4.2),(4.4),(4.5) as follow:

$E^d_{i(V)}(q_1)$ and $E^d_{i(V)}(q_2)$ are the defects formation energies at $E_F = 0$ and charge states q_1 and q_2. The values of $E^d_{i(V)}(q)$ are obtained from $E_{f,avg}$ in the last column of Table 4.5 for charged (with charges +2, -2, +1, and -1) and neutral (0 charge) defects. The values of $\mu_{i(V)}(q_1,q_2){\equiv}\mu_{semilocal}$ are shown in the first column of Table 4.6 where (0, -2), (+2, 0), (+1, 0), and (0, -1) are the charge transitions (q_1, q_2) for, respectively, Ca vacancy (Ca$_v$), Ca interstitial (Ca$_i$), F vacancy (F$_v$), and F interstitial (F$_i$). $\mu_{semilocal}$ are the values before the correction for the error arising from the band gap underestimation. The correction factor δ = VBM$_{PBE0}$ – VBM$_{PBE}$ ~ 2 eV (figure. 4.11) can be added to $\mu_{semilocal}$ to place the level in the corrected band gap, E^{PBE0}_g ~ 10.6 eV (see figure 4.11b), associated with the PBE0 calculation. The corrected values $\mu_{corrected} = \mu_{semilocal}$ + δ are listed in the second column of Table 4.6. It is clear that $\mu_{corrected}$ are given with reference to the VBM$_{PBE0}$ and, hence, falling within the corrected band gap E^{PBE0}_g (figure 4.11a). On the other hand $\mu_{semilocal}$ are given with respect to VBM$_{PBE}$ (figure 4.11b).

The above procedure of correcting the level positions follows tightly the correction recipe suggested in Ref[39]. The condition for implementing this recipe is that VBM$_{PBE0}$ and VBM$_{PBE}$ (figure.4.11) must be given with reference to a common ionic electrostatic potential. Satisfying this condition leads to the alignment of $\mu_{corrected}$ and $\mu_{semilocal}$ as demonstrated in Ref[39]. Such condition is true in our case since the QE calculations in figure 4.11 are based on the same pseudopotentials. Additionally the default energy scale in QE software is set

relative to the ionic electrostatic potential. In other words the energy scale in figure 4.11 for the QE data is automatically given with respect to the ionic electrostatic potential. That is why the w2k NDOS (figure 4.2) are manually shifted to align with that from QE calculation since the main purpose of the w2k data is to optimize the band gap size.

Table 4.6: The correction of the transition levels ($\mu_{semilocal}$) from semilocal calculation using the correction factor $\delta = VBM_{PBE0} - VBM_{PBE} \sim 2$ eV in figure 4.12. $\mu_{semilocal}$ is given with respect to VBM_{PBE0}.

Defect	Charge transition	$\mu_{semilocal}$ (eV)	$\mu_{corrected}$ (eV) $= \mu_{semilocal} + \delta$
Ca_v	(0, -2)	0.40	2.40
Ca_i	(+2, 0)	6.65	8.56
F_v	(+1, 0)	5.83	7.83
F_i	(0, − 1)	0.30	2.30

From table 4.3 and tabe 4.6 we can conclude that the transiton levels of the barium Fluorides is similar to those for Calcium Flouride and this is due to their cubic compound structure ,besides the similarity in their properties.

CHAPTER FIVE

CONCLUSION AND FUTURE WORK

5.1CONCLUSION

We have managed to calculate with high accuracy the charge transition levels of stable native defects in two of the fluorite structures, BaF2 and CaF2, using advanced first-principle calculation methods. After a thorough literature survey we recognized that such kind of investigation was lacking apart from a timely report by Nyawere et al about the identification of stable native defects in BaF2. This study has clearly illuminated the importance of accurate native defect levels for the technology and fundamental Physics specially after arriving at a value for the F-center level that was close to the experimental one obtained by optical absorption band method. Furthermore, the study has demonstrated that these wide gap fluorite structures could facilitate advanced investigation associated with the localized electronic wave function interactions between defects without sever interaction with the band states, rendering these materials as prototypes for fundamental studies of the physics of defect and isolated atoms.

The transition level was assigned to the Fermi level where two defect charge states have the same formation energy. The error in the calculation of the formation energies arising from image charge interactions between periodic supercells have been relieved using Makov-Payne correction factor.Semilocal and hybrid density-functional calculations are performed, as described by Alkauskaset al (PRL 101, 046405 (2008)), in order to accurately place the transition levels, relative to the valence band maximum, in the corrected band

gap of BaF2 and CaF2. Finally, full-potential, Linearized Augmented Planewave calculation, known for its accuracy, is performed to validate the band gaps from the semilocal and hybrid calculations.

We also find that the charged cation in Barium Flouride is the most stable native defect than the encountered on in Calcium fluoride.More over we found that the transition levels of Barium Flouride are similar to those in Calcium Flouride.

The results in figure (4.11a) and figure (4.11b) show three important points. First, GGA always over estimated the cell parameters, and the LDA was accurate in determining the cell parameters when using pbe0 pseudopotential. However, LDA under estimated the cell parameters when using the ultrasoft pseudopotential. Generally the universal feature of the LDA and GGA should be that the LDA tends to underestimate lattice parameters, which are then corrected by the GGA to values closer to the experimental results. However, we also found that the under estimation /overestimation of lattice parameter also depends on the pseudopotentials used in the calculations. For example, when using the norm-conserving pseudoopotential, both the LDA and GGA overestimated the lattice parameters, although the parameters in LDA calculation was just slightly overestimated. Secondly, the calculations using ultrasoftpseudopotential (usp) with the LDA and real space were not well converged comparing with the other cases. The use of ultrasoft pseudopotentials were acceptable only in reciprocal space. The best choice of approximations for use in our study is the combination of GGA + ultrasoftpseudopotential.

The mBJLDA methods gives rise to acceptable predictions of the band gap value as compared to experiment,but this method is highly computational cost. If one would seek for precision without taking this factor into account, the quantum espresso is the method to use. If one wouldprefer to sacrifice a little the precision obtained against the savings in computational cost, the mBJLDA seems the appropriate method. In conclusion, we can typify the state of matters

with respect to the calculation of the band gap of MF2 as follows,A quite precise method does exist, the quantum espresso simulations package,It's computational cost is lower. A relatively quicker code, theWien2k implemented with the mBJLDA potential, gives somehow more accurate results than the other.

5.2 Future work

From here, there are many possible avenues that future work can take. For the transition level study in barium fluoride and calcium fluoride. There is a natural place to continue; now that we know the important defects to consider we can start looking for suitable dopants to obtain an n-type material and study their optical and electronic properties. Modern methods are still primarily in the realm of developing a huge database of potential dopants and then data mining the result for the proper energetic and effect on band structure. On a personal level, it is discouraging that this scattershot approach is the most sophisticated means of solving this problem, but it also should not be surprising as this is what the computer really does best. The art in this work is to prioritize the most likely candidate materials as well as determine how to preserve the most relevant physics in our calculations (such as choice of which pesudopotentials to use).More over we can use other sophisticated software for matter of comparative such as VASP simulation package known with it is accuracy in calculating band gab as well as wein2k software.

It is very crucial to conduct further study on accuracy of hybrid functional applying on calculating the defect formation energies of Alkaline earth fluorides structure.

It will be useful to perform the same techniques (extrapolations methods and potential alignment) to the reminder of the alkaline earth fluorides (SrF_2, MgF_2) in order to have Comparative studies about their electronic properties ,formation energies, and transition levels.

REFERENCES

[1]. Rubloff, G.W., Far-ultraviolet reflectance spectra and the electronic structure of ionic crystals. Physical Review B, 1972. 5(2): p. 662.

[2]. Laval, M., et al., Barium fluoride—inorganic scintillator for subnanosecond timing. Nuclear Instruments and Methods in Physics Research, 1983. 206(1): p. 169-176.

[3]. Burnett, J.H., Z.H. Levine, and E.L. Shirley, Intrinsic birefringence in calcium fluoride and barium fluoride. Physical Review B, 2001. 64(24): p. 241102.

[4]. Nyawere, P.W.O., et al., Ab-initio calculation of formation and migration energies of intrinsic defects in BaF_2. Solid state communications, 2014. 179: p. 25-28

[5]. Puchina, A., et al., Ab initio study of the F centers in CaF_2: Calculations of the optical absorption, diffusion and binding energies. Solid state communications, 1998. 106(5): p. 285-288.

[6]. Verstraete, M. and X. Gonze, First-principles calculation of the electronic, dielectric, and dynamical properties of CaF_2. Physical Review B, 2003. 68(19): p. 195123.

[7]. Sata, N., et al., Mesoscopic fast ion conduction in nanometre-scale planar heterostructures. Nature, 2000. 408(6815): p. 946-949.

[8]. Robinson, M., et al., Infrared-transparent glasses derived from the fluorides of zirconium, thorium, and barium. Materials Research Bulletin, 1980. 15(6): p. 735-742.

[9]. Zhu, R.-Y., On quality requirements to the barium fluoride crystals. Nuclear Instruments and Methods in Physics Research Section A: Accelerators, Spectrometers, Detectors and Associated Equipment, 1994. 340(3): p. 442-457.

[10]. Dressler, L., R. Rauch, and R. Reimann, On the Inhomogeneity of Refractive Index of CaF2 Crystals for High Performance Optics. Crystal Research and Technology, 1992. 27(3): p. 413-420.

[11]. Shimizu, Y., et al., Dark matter search experiment with CaF_2 (Eu) scintillator at Kamioka Observatory. Physics Letters B, 2006. 633(2): p. 195-200.

[12]. Parr, R.G. and W. Yang, Density-functional theory of atoms and molecules. Vol. 16. 1989: Oxford university press.

[13]. Foster, A., T. Trevethan, and A. Shluger, Structure and diffusion of intrinsic defects, adsorbed hydrogen, and water molecules at the surface of alkali-earth fluorides calculated using density functional theory. Physical Review B, 2009. 80(11): p. 115421.

[14]. Shi, H., R. Eglitis, and G. Borstel, Ab initio calculations of the BaF_2 bulk and surface F centres. Journal of Physics: Condensed Matter, 2006. 18(35): p. 8367.

[15]. Aryasetiawan, F. and O. Gunnarsson, The GW method. Reports on Progress in Physics, 1998. 61(3): p. 237.

[16]. Nyawere, P., N. Makau, and G. Amolo, First-principles calculations of the elastic constants of the cubic, orthorhombic and hexagonal phases of BaF 2. Physica B: Condensed Matter, 2014. 434: p. 122-128

[17]. Grimme, S., Semiempirical hybrid density functional with perturbative second-order correlation. The Journal of chemical physics, 2006. 124(3): p. 034108.

[18]. Perdew, J.P., K. Burke, and M. Ernzerhof, Generalized gradient approximation made simple. Physical review letters, 1996. 77(18): p. 3865.

[19]. Alkauskas, A., P. Broqvist, and A. Pasquarello, Defect energy levels in density functional calculations: Alignment and band gap problem. Physical review letters, 2008. 101(4): p. 046405.

[20]. Hohenberg, P. and W. Kohn, Inhomogeneous electron gas. Physical review, 1964. 136(3B): p. B864.

[21]. Kohn, W. and L.J. Sham, Self-consistent equations including exchange and correlation effects. Physical Review, 1965. 140(4A): p. A1133.

[22]. Feynman, R.P. and L.M. Brown, Selected papers of Richard Feynman: with commentary. Vol. 27. 2000: World Scientific.

[23]. Martin, R.M., Electronic Structure : Basic Theory And Practical Methods 2004, Cambridge ; New York: Cambridge University press. xxiii, 624 p.

[24]. Johnson, D.D., Modified Broyden's method for accelerating convergence in self-consistent calculations. Physical Review B, 1988. 38(18): p. 12807.

[25]. Kresse, G. and J. Furthmüller, Efficient iterative schemes for ab initio total-energy calculations using a plane-wave basis set. Physical Review B, 1996. 54(16): p. 11169.

[26]. Dirac, P.A. Note on exchange phenomena in the Thomas atom. in Mathematical Proceedings of the Cambridge Philosophical Society. 1930: Cambridge Univ Press.

[27]. Becke, A.D., Density-functional exchange-energy approximation with correct asymptotic behavior. Physical review A, 1988. 38(6): p. 3098.

[28]. Perdew, J.P., et al., MR, Pederson, DJ Singh, C. Fiolhais. Phys. Rev. B, 1992. 46(24): p. 6671.

[29]. Perdew, J., K. Burke, and M. Ernzerhof, Phys Rev Lett 77: 3865. Errata:(1997) Phys Rev Lett, 1996. 78: p. 1396.

[30]. Perdew, J.P. and M. Levy, Physical content of the exact Kohn-Sham orbital energies: band gaps and derivative discontinuities. Physical Review Letters, 1983. 51(20): p. 1884.

[31]. Becke, A.D., A new mixing of Hartree–Fock and local density-functional theories. The Journal of Chemical Physics, 1993. 98(2): p. 1372-1377.

[32]. Kim, K. and K. Jordan, Comparison of density functional and MP2 calculations on the water monomer and dimer. The Journal of Physical Chemistry, 1994. 98(40): p. 10089-10094.

[33]. Stephens, P., et al., Ab initio calculation of vibrational absorption and circular dichroism spectra using density functional force fields. The Journal of Physical Chemistry, 1994. 98(45): p. 11623-11627.

[34]. Zaanen, J., et al., Physica C 153-155, 1636 (1988); VI Anisimov, J. Zaanen, and OK Andersen. Phys. Rev. B, 1991. 44: p. 943.

[35]. Hedin, L., New method for calculating the one-particle Green's function with application to the electron-gas problem. Physical Review, 1965. 139(3A): p. A796.

[36]. Aulbur, W.G., L. Jönsson, and J.W. Wilkins, Quasiparticle calculations in solids. Solid State Physics, 2000. 54: p. 1-218.

[37]. Heyd, J., G.E. Scuseria, and M. Ernzerhof, Erratum:"Hybrid functionals based on a screened Coulomb potential"[J. Chem. Phys. 118, 8207 (2003)]. The Journal of Chemical Physics, 2006. 124(21): p. 219906.

[38]. Henderson, T., AF izmaylov, GE Scuseria, and A. J. Theor. Comput. Chem, 2008. 4: p. 1254.

[39]. Tran, F. and P. Blaha, Accurate band gaps of semiconductors and insulators with a semilocal exchange-correlation potential. Physical Review Letters, 2009. 102(22): p. 226401.

[40]. Dixit, H., et al., Electronic structure of transparent oxides with the Tran–Blaha modified Becke–Johnson potential. Journal of Physics: Condensed Matter, 2012. 24(20): p. 205503.

[41].Monkhorst, H.J. and J.D. Pack, Special points for Brillouin-zone integrations. Physical Review B, 1976. 13(12): p. 5188.

[42]. Schwerdtfeger, P., The pseudopotential approximation in electronic structure theory. ChemPhysChem, 2011. 12(17): p. 3143-3155.

[43]. Vanderbilt, D., Soft self-consistent pseudopotentials in a generalized eigenvalue formalism. Physical Review B, 1990. 41(11): p. 7892.

[44]. Blöchl, P.E., Projector augmented-wave method. Physical Review B, 1994. 50(24): p. 17953.

[45]. Kresse, G. and D. Joubert, From ultrasoft pseudopotentials to the projector augmented-wave method. Physical Review B, 1999. 59(3): p. 1758.

[46]. Giannozzi, P., et al., QUANTUM ESPRESSO: a modular and open-source software project for quantum simulations of materials. Journal of Physics: Condensed Matter, 2009. 21(39): p. 395502.

[47]. Jones, R. and P. Briddon, The ab initio cluster method and the dynamics of defects in semiconductors. Identification of Defects in Semiconductors, 1998. 51: p. 287.

[48]. PY Yu and M. Cardona, Fundamentals of Semiconductors; Physics and Materials Properties, Springer-Verlag, Berlin and Heidelberg, 1996, 617p., 15.4× 23.5 cm, 7,481.

[49]. Drabold, D.A. and S.K. Estreicher, Defect theory: An armchair history. 2007: Springer.

[50]. Alkauskas, A., et al., Advanced Calculations for Defects in Materials: Electronic Structure Methods. 2011: John Wiley & Sons.

[51]. Schottky, W., Über den Mechanismus der Ionenbewegung in festen Elektrolyten. Zeitschrift der physikalischen Chemie (Band B 29), 1935: p. 335-355.

[52]. Arends, J., Color centers in additively colored CaF2 and BaF2. physica status solidi (b), 1964. 7(3): p. 805-815.

[53]. Den Hartog, H. and J. Arends, F-Centers in SrF2. physica status solidi (b), 1967. 22(1): p. 131-140.

[54]. Nepomnyashchikh, A., et al., Defect formation and VUV luminescence in BaF 2. Radiation effects and defects in solids, 2002. 157(6-12): p. 715-719.

[55]. Hayes, W., Crystals with the fluorite structure. 1974: Clarendon Press.

[56]. Becke, A.D. and K.E. Edgecombe, A simple measure of electron localization in atomic and molecular systems. The Journal of chemical physics, 1990. 92(9): p. 5397-5403.

[57]. Flynn, C.P., Point defects and diffusion. 1972.

[58]. Reif, F., Statistical thermal physics. 1965: Mcgraw-Hill Kogakusha.

[59]. Van de Walle, C.G. and J. Neugebauer, First-principles calculations for defects and impurities: Applications to III-nitrides. Journal of Applied Physics, 2004. 95(8): p. 3851-3879.

[60]. Hagen, M. and M.W. Finnis, Point defects and chemical potentials in ordered alloys. Philosophical Magazine A, 1998. 77(2): p. 447-464.

[61]. Makov, G. and M. Payne, Periodic boundary conditions in ab initio calculations. Physical Review B, 1995. 51(7): p. 4014.

[62]. Broqvist, P., A. Alkauskas, and A. Pasquarello, Hybrid-functional calculations with plane-wave basis sets: Effect of singularity correction on total energies, energy eigenvalues, and defect energy levels. Physical Review B, 2009. 80(8): p. 085114.

[63]. Alkauskas, A., P. Broqvist, and A. Pasquarello, Defect levels through hybrid density functionals: Insights and applications. physica status solidi (b), 2011. 248(4): p. 775-789.

[64]. Ihm, J., A. Zunger, and M.L. Cohen, Momentum-space formalism for the total energy of solids. Journal of Physics C: Solid State Physics, 1979. 12(21): p. 4409.

[65]. Robinson, M., et al., Infrared-transparent glasses derived from the fluorides of zirconium, thorium, and barium. Materials Research Bulletin, 1980. 15(6): p. 735-742.

[66]. Monkhorst, H.J. and J.D. Pack, Special points for Brillouin-zone integrations. Physical Review B, 1976. 13(12): p. 5188.

[67]. Hellmann, H., Einfuhrung in die Quantumchemie. Franz Deutsche, Leipzig, 1937: p. 285.

[68]. Feynman, R.P., Forces in molecules. Physical Review, 1939. 56(4): p. 340.

[69]. Sedaghati, R., A. Suleman, and B. Tabarrok, Structural optimization with frequency constraints using the finite element force method. AIAA journal, 2002. 40(2): p. 382-388.

[70]. Poirier, J.-P. and A. Tarantola, A logarithmic equation of state. Physics of the Earth and Planetary Interiors, 1998. 109(1): p. 1-8.

[71]. Srinivasan, R., Lattice Theory of the Elastic Dielectric: Application to the Fluorite Lattice. Physical Review, 1968. 165(3): p. 1054.

[72]. Stewart, J.J., MOPAC: a semiempirical molecular orbital program. Journal of computer-aided molecular design, 1990. 4(1): p. 1-103.

[73]. Shi, H., R. Eglitis, and G. Borstel, Ab initio calculations of the Ca F 2 electronic structure and F centers. Physical Review B, 2005. 72(4): p. 045109.

[74]. Hamann, D., M. Schlüter, and C. Chiang, Norm-conserving pseudopotentials. Physical review letters, 1979. 43(20): p. 1494.

[75]. Seidl, A., et al., Generalized Kohn-Sham schemes and the band-gap problem. Physical Review B, 1996. 53(7): p. 3764.

[76]. Makov, G. and M. Payne, Periodic boundary conditions in ab initio calculations. Physical Review B, 1995. 51(7): p. 4014.

[77]. Lany, S. and A. Zunger, Assessment of correction methods for the band-gap problem and for finite-size effects in supercell defect calculations: Case studies for ZnO and GaAs. Physical Review B, 2008. 78(23): p. 235104.

Main Publications

1. **A.M.Ibraheem** .Effect of Radiation on the properties of ZnO Films and Substrates. International Journal of Science and Research(IJSR) ISSN(online):2319-7064

2. **A. M. Ibraheem** , A. E. Elfaki, and M. A. H. Khalafalla

Firt principle calculations of formation energies stability of native defects on CaF_2 .International Journal of Science and Research(IJSR) ART2016708

Appendices

Appendix A

EXAMPLE OF QUANTUM-ESPRESSO INPUT FILES

```
#!/bin/sh

# run from directory where this script is

cd `echo $0 | sed 's/\(.*\)\/.*/\1/'` # extract pathname

EXAMPLE_DIR=`pwd`

# check whether echo has the -e option

if test "`echo -e`" = "-e" ; then ECHO=echo ; else ECHO="echo -e" ; fi

# function to test the exit status of a job

$ECHO

$ECHO "$EXAMPLE_DIR : starting"

$ECHO

$ECHO "This example shows how to use pw.x to calculate the total energy and"

$ECHO "the band structure of four simple systems: Si, Al, Cu, Ni."

# set the needed environment variables

. ./environment_variables

# required executables and pseudopotentials
```

```
BIN_LIST="pw.xdos.x"

PSEUDO_LIST="S.pz-n-rrkjus_psl.0.1.UPF        In.pz-dn-rrkjus_psl.0.2.2.UPF
S.rel-pz-n-kjpaw_psl.0.1.UPF In.rel-pz-dn-kjpaw_psl.0.2.2.UPF"

$ECHO

$ECHO "  executables directory: $BIN_DIR"

$ECHO "  pseudo directory:      $PSEUDO_DIR"

$ECHO "  temporary directory:   $TMP_DIR"

$ECHO "  checking that needed directories and files exist...\c"

# check for directories

for DIR in "$BIN_DIR" "$PSEUDO_DIR" ; do

if test ! -d $DIR ; then

    $ECHO

    $ECHO "ERROR: $DIR not existent or not a directory"

    $ECHO "Aborting"

exit 1

fi

done

for DIR in "$TMP_DIR" "$EXAMPLE_DIR/results96_dos" ; do

if test ! -d $DIR ; then

mkdir $DIR
```

```
fi

done

cd $EXAMPLE_DIR/results96_dos

# check for executables

for FILE in $BIN_LIST ; do

if test ! -x $BIN_DIR/$FILE ; then

    $ECHO

    $ECHO "ERROR: $BIN_DIR/$FILE not exist

istent or not executable"

    $ECHO "Aborting"

exit 1

fi

done

# how to run executables

PW_COMMAND="$PARA_PREFIX $BIN_DIR/pw.x $PARA_POSTFIX"

DOS_COMMAND="$PARA_PREFIX $BIN_DIR/dos.x $PARA_POSTFIX"

$ECHO

$ECHO "  runningpw.x as: $PW_COMMAND"

$ECHO "  runningdos.x as: $DOS_COMMAND"
```

```
$ECHO

 # clean TMP_DIR

   $ECHO "  cleaning $TMP_DIR...\c"

rm -rf $TMP_DIR/*

   $ECHO " done"

 # band structure calculation along delta, sigma and lambda lines

cat> CaF96.in << EOF

&control

calculation='scf',

restart_mode='from_scratch',

pseudo_dir='$PSEUDO_DIR/',

outdir = '$TMP_DIR/',

prefix='CaF1'

etot_conv_thr= 1.0D-4,

forc_conv_thr= 1.0D-3

 /

&system

ibrav= 0, A= 1, nat=96, ntyp= 2, ecutwfc =40.0

 /
```

&electrons

mixing_beta = 0.5D0,

conv_thr   = 1.D-6

/

ATOMIC_SPECIES

Ca40.078 ca_pbe_v1.uspp.F.UPF

 F 18.998404 f_pbe_v1.4.uspp.F.UPF

ATOMIC_POSITIONS {angstrom}

Ca 0.000000000   0.000000000   0.000000000

Ca 0.000000000   2.731604576   2.731604576

Ca 2.731604576   0.000000000   2.731604576

Ca 2.731604576   2.731604576   0.000000000

Ca 0.000000000   0.000000000   5.463209152

Ca 5.463209152   0.000000000   0.000000000

Ca 0.000000000   5.463209152   0.000000000

Ca 0.000000000   2.731604576   8.194813728

Ca 5.463209152   2.731604576   2.731604576

Ca 0.000000000   8.194813728   2.731604576

Ca 2.731604576   0.000000000   8.194813728

Ca 8.194813728   0.000000000   2.731604576

Ca 2.731604576   5.463209152   2.731604576

Ca 2.731604576   2.731604576   5.463209152

Ca 8.194813728   2.731604576   0.000000000

Ca 2.731604576   8.194813728   0.000000000

Ca 0.000000000   5.463209152   5.463209152

Ca 5.463209152   0.000000000   5.463209152

Ca 5.463209152   5.463209152   0.000000000

Ca 0.000000000   8.194813728   8.194813728

Ca 5.463209152   2.731604576   8.194813728

Ca 5.463209152   8.194813728   2.731604576

Ca 2.731604576   5.463209152   8.194813728

Ca 8.194813728   0.000000000   8.194813728

Ca 8.194813728   5.463209152   2.731604576

Ca 2.731604576   8.194813728   5.463209152

Ca 8.194813728   2.731604576   5.463209152

Ca 8.194813728   8.194813728   0.000000000

Ca 5.463209152   5.463209152   5.463209152

Ca 5.463209152   8.194813728   8.194813728

Ca 8.194813728   5.463209152   8.194813728

Ca 8.194813728   8.194813728   5.463209152

F 1.365802288   1.365802288   1.365802288

F 9.560616016   9.560616016   9.560616016

F 9.560616016   9.560616016   1.365802288

F 1.365802288   1.365802288   9.560616016

F 9.560616016   1.365802288   9.560616016

F 1.365802288   9.560616016   1.365802288

F 1.365802288   9.560616016   9.560616016

F 9.560616016   1.365802288   1.365802288

F 1.365802288   4.097406864   4.097406864

F 9.560616016   1.365802288   4.097406864

F 1.365802288   4.097406864   1.365802288

F 9.560616016   4.097406864   1.365802288

F 1.365802288   1.365802288   4.097406864

F 9.560616016   4.097406864   4.097406864

F 4.097406864   1.365802288   4.097406864

F 1.365802288   9.560616016   4.097406864

F 4.097406864   1.365802288   1.365802288

F 4.097406864   9.560616016   4.097406864

F 4.097406864   9.560616016   1.365802288

F 4.097406864   4.097406864   1.365802288

F 4.097406864   4.097406864   9.560616016

F 1.365802288   4.097406864   9.560616016

F 4.097406864   1.365802288   9.560616016

F 1.365802288   1.365802288   6.829011440

F 9.560616016   9.560616016   4.097406864

F 9.560616016   9.560616016   6.829011440

F 1.365802288   9.560616016   6.829011440

F 9.560616016   1.365802288   6.829011440

F 6.829011440   1.365802288   1.365802288

F 4.097406864   9.560616016   9.560616016

F 6.829011440   9.560616016   9.560616016

F 6.829011440   1.365802288   9.560616016

F 6.829011440   9.560616016   1.365802288

F 1.365802288   6.829011440   1.365802288

F 9.560616016   4.097406864   9.560616016

F 9.560616016   6.829011440   9.560616016

F 9.560616016   6.829011440   1.365802288

F 1.365802288   6.829011440   9.560616016

F 1.365802288   4.097406864   6.829011440

F 9.560616016   4.097406864   6.829011440

F 6.829011440   4.097406864   4.097406864

F 4.097406864   4.097406864   4.097406864

F 6.829011440   4.097406864   1.365802288

F 6.829011440   1.365802288   4.097406864

F 1.365802288   6.829011440   4.097406864

F 9.560616016   6.829011440   4.097406864

F 4.097406864   1.365802288   6.829011440

F 4.097406864   9.560616016   6.829011440

F 6.829011440   9.560616016   4.097406864

F 4.097406864   6.829011440   4.097406864

F 4.097406864   6.829011440   1.365802288

F 4.097406864   4.097406864   6.829011440

F 6.829011440   4.097406864   9.560616016

F 4.097406864   6.829011440   9.560616016

F 1.365802288   6.829011440   6.829011440

```
F  9.560616016        6.829011440        6.829011440

F  6.829011440        1.365802288        6.829011440

F  6.829011440        9.560616016        6.829011440

F  6.829011440        6.829011440        1.365802288

F  6.829011440        6.829011440        9.560616016

F  6.829011440        4.097406864        6.829011440

F  6.829011440        6.829011440        4.097406864

F  4.097406864        6.829011440        6.829011440

F  6.829011440        6.829011440        6.829011440
K_POINTS  gamma

CELL_PARAMETERS alat

10.9264183044        0.0000000000        0.0000000000

 0.0000000000       10.9264183044        0.0000000000

 0.0000000000        0.0000000000       10.9264183044
EOF

$ECHO "  running the scf calculation for Si...\c"

$PW_COMMAND < CaF96.in > CaF96.out

  $ECHO " done"

  #clean TMP_DIR
```

```
$ECHO "  cleaning $TMP_DIR...\c"

rm -rf $TMP_DIR/*

  $ECHO " done".
```

Appendix B

QUANTUM ESPRESSO –HYBRID FILE OF (BaF$_2$)

```sh
#!/bin/sh


# run from directory where this script is

cd `echo $0 | sed 's/\(.*\)\/.*/\1/'` # extract pathname

EXAMPLE_DIR=`pwd`


# check whether echo has the -e option

if test "`echo -e`" = "-e" ; then ECHO=echo ; else ECHO="echo -e" ; fi


$ECHO

$ECHO "$EXAMPLE_DIR : starting"

$ECHO

$ECHO "This example shows how to use pw.x to calculate the total energy"

$ECHO "of silicon and of a few small molecules using hybrid functionals."


# set the needed environment variables

. ../environment_variables


# required executables and pseudopotentials

BIN_LIST="pw.x"

PSEUDO_LIST="Si.pz-vbc.UPF"
```

```
x_gamma_extrapolation=".TRUE."

exxdiv_treatment="gygi-baldereschi"

if [ ! -z "$1" ] ; then exxdiv_treatment="$1" ; fi

if [ "$exxdiv_treatment" = "vcut_ws" ] ; then x_gamma_extrapolation=.FALSE.
; fi

if [ "$exxdiv_treatment" = "vcut_spherical" ] ; then
x_gamma_extrapolation=.FALSE. ; fi

ecutvcut=0.7


$ECHO

$ECHO "  executables directory: $BIN_DIR"

$ECHO "  pseudo directory:      $PSEUDO_DIR"

$ECHO "  temporary directory:   $TMP_DIR"

$ECHO "  checking that needed directories and files exist...\c"


# check for directories
for DIR in "$BIN_DIR" "$PSEUDO_DIR" ; do
   if test ! -d $DIR ; then
      $ECHO
      $ECHO "ERROR: $DIR not existent or not a directory"
      $ECHO "Aborting"
      exit 1
   fi
done
```

```
for DIR in "$TMP_DIR" "$EXAMPLE_DIR/results/BaF_hyb" ; do

    if test ! -d $DIR ; then

        mkdir $DIR

    fi

done

cd $EXAMPLE_DIR/results/BaF_hyb


# check for executables

for FILE in $BIN_LIST ; do

    if test ! -x $BIN_DIR/$FILE ; then

        $ECHO

        $ECHO "ERROR: $BIN_DIR/$FILE not existent or not executable"

        $ECHO "Aborting"

        exit 1

    fi

done


# check for pseudopotentials

for FILE in $PSEUDO_LIST ; do

    if test ! -r $PSEUDO_DIR/$FILE ; then

        $ECHO

        $ECHO "Downloading $FILE to $PSEUDO_DIR...\c"

            $WGET $PSEUDO_DIR/$FILE $NETWORK_PSEUDO/$FILE 2>
/dev/null

    fi
```

```
  if test $? != 0; then

     $ECHO

     $ECHO "ERROR: $PSEUDO_DIR/$FILE not existent or not readable"

     $ECHO "Aborting"

     exit 1

  fi

done

$ECHO " done"


# how to run executables

PW_COMMAND="$PARA_PREFIX $BIN_DIR/pw.x $PARA_POSTFIX"

DOS_COMMAND="$PARA_PREFIX $BIN_DIR/dos.x $PARA_POSTFIX"

$ECHO

$ECHO "  running pw.x as: $PW_COMMAND"

$ECHO


$ECHO

$ECHO "  running PBE0 calculation for Si with nq=1,2,4 \c"

$ECHO


#for nq in 1 2 4; do


# self-consistent calculation

rm -rf $TMP_DIR/*
```

```
cat > BaF_scf_hyb.in << EOF
 &control
    calculation = 'scf'
    restart_mode='from_scratch',
    prefix='baf_hyb',
    pseudo_dir = '$PSEUDO_DIR/',
    outdir='$TMP_DIR/'
 /
 &system
    ibrav=  0, A = 6.20010, nat=  3, ntyp= 2,
    ecutwfc =15.0, occupations='tetrahedral',
    input_dft='pbe0',
    ecutvcut=$ecutvcut
    x_gamma_extrapolation = $x_gamma_extrapolation
 /
 &electrons
    mixing_beta = 0.7
    conv_thr =  1.0d-3
 /
CELL_PARAMETERS {alat}
 0.500000000000000  0.500000000000000  0.000000000000000
 0.500000000000000  0.000000000000000  0.500000000000000
 0.000000000000000  0.500000000000000  0.500000000000000
ATOMIC_SPECIES
```

```
 Ba 137.32700 Ba.pz-hgh.UPF

 F 18.99800 F.pz-hgh.UPF

ATOMIC_POSITIONS

 Ba  0.000000000000000  0.000000000000000  0.000000000000000

 F  0.250000000000000  0.250000000000000  0.250000000000000

 F  0.750000000000000  0.750000000000000  0.750000000000000

K_POINTS {automatic}

1 1 1 0 0 0

EOF

$ECHO "  running the scf calculation for Si with nq = 4 ...\c"

$PW_COMMAND < BaF_scf_hyb.in > BaF_scf_hyb.out

$ECHO " done"

grep -e ! BaF_scf_hyb.out | tail -1

#

#DOS calculation

cat > BaF_dos_hyb.in << EOF

&DOS

prefix='baf_hyb'

outdir = '$TMP_DIR',

DeltaE=0.001,

fildos='BaF_dos_hyb.dos',

  /

EOF

$ECHO "  running the scf calculation for Si...\c"
```

```
$DOS_COMMAND <BaF_dos_hyb.in> BaF_dos_hyb.out

$ECHO " done"

#

#

#done

# clean TMP_DIR

#$ECHO "  cleaning $TMP_DIR...\c"

#rm -rf $TMP_DIR/barium*

$ECHO " done"
```